Modeling and analysis of voltage-dependent photo and dark current characteristics of Bulk Heterojunction organic solar cells

Md Mesbahus Saleheen

A Thesis

in

the Department

of

Electrical and Computer Engineering

Presented in Partial Fulfillment of the Requirement

for the Degree of Master of Applied Science at

Concordia University

Montréal, Québec, Canada

June 2016

CONCORDIA UNIVERSITY
SCHOOL OF GRADUATE STUDIES

This is to certify that the thesis prepared

By: Md. Mesbahus Saleheen

Entitled: "Modeling and Analysis of Voltage-dependent Photo and Dark Current Characteristics of Bulk Heterojunction Organic Solar Cells"

and submitted in partial fulfillment of the requirements for the degree of

Master of Applied Science

Complies with the regulations of this University and meets the accepted standards with respect to originality and quality.

Signed by the final examining committee:

_____ Chair
Dr. R. Raut

_____ Examiner, External
Dr. A. Bhowmick, BCEE To the Program

_____ Examiner
Dr. P. Valizadeh

_____ Supervisor
Dr. M. Z. Kabir

Approved by: _____
Dr. W. E. Lynch, Chair
Department of Electrical and Computer Engineering

_____20_____ _____
Dr. Amir Asif, Dean
Faculty of Engineering and Computer Science

ABSTRACT

Modeling and analysis of voltage-dependent photo and dark current characteristics of Bulk Heterojunction organic solar cells.

Md Mesbahus Saleheen

Over the past decade, bulk heterojunction (BHJ) polymer solar cells based on blends of conjugated polymers and fullerene derivatives (e.g., P3HT:PCBM blend) have drawn a huge attention in research due to their high conversion efficiency, solution-based easy fabrication, and abundant availability. Although presently BHJ cells show a reasonable power conversion efficiency (almost 10 %), further efficiency improvements/optimizations seem very likely by better understanding the operating principles through accurate physics-based modeling and optimizations.

In this thesis, a physics-based explicit mathematical model for the external voltage-dependent forward dark current in bulk heterojunction (BHJ) organic solar cells is developed by considering Shockley-Read-Hall (SRH) recombination and solving the continuity equations for both electrons and holes with proper boundary conditions. An analytical model for the external voltage-dependent photocurrent in BHJ organic solar cells is also proposed by incorporating exponential photon absorption, dissociation efficiency of bound electron-hole pairs (EHPs), carrier trapping, and carrier drift and diffusion in the photon absorption layer. Modified Braun's model is used to compute the electric field-dependent dissociation efficiency of the bound EHPs. The overall net current is calculated considering the actual solar spectrum. The mathematical models are verifield by comparing the model calculations with various published experimental results. We analyze the effects of the contact properties, blend compositions, charge carrier transport properties (carrier mobility and lifetime), and cell design on the current-voltage characteristics. The power conversion efficiency of BHJ organic solar cells mostly depends on electron transport properties (both the mobility and lifetime) of the acceptor layer. The results of this paper indicate that improvement of charge carrier transport (both mobility and lifetime) and dissociation of bound EHPs in organic blend are critically important to increase the power conversion efficiency of the BHJ solar cells.

ACKNOWLEDGEMENT

All praises belong to Almighty who gave me the health, strength and ability to complete my thesis.

I would like to express my deepest gratitude to my supervisor Dr. Zahangir Kabir for his encouragement, helpful advice, discussion, guidance and financial support throughout these years.

I am very grateful to all of my family members who supported me mentally over the past two years.

Finally, I would like to give special thanks to Salman Moazzem Arnab and Kaveh Rahbardar Mojaver for their great assistance. I am also grateful to other research members named Nour Hijazi, Sinchita Siddiquee and Dhilippan M P.

TABLE OF CONTENTS

LIST OF FIGURES

LIST OF TABLES

LIST OF ABBREVIATION

AgBr	-	Silver bromide
AgCl	-	Silver chloride
AM	-	Air mass
BHJ	-	Bulk heterojunction
CB	-	Conduction band
EHP	-	Electron and hole pair
EQE	-	External quantum efficiency
FF	-	Fill factor
HOMO	-	Highest occupied molecular orbital
ITO	-	Indium tin oxide
LUMO	-	Lowest unoccupied molecular orbital
OSC	-	Organic solar cell
P3HT	-	Poly(3-hexylthiophene)
PCBM	-	[6,6]-phenyl C_{61}-butyric acid methyl ester
PCE	-	Power conversion efficiency
PEDOT:PSS	-	Poly(3,4-ehylenedioxythiophene):poly(styrenesulfonate)
Pt	-	Platinum
PTB7	-	Polythieno[3,4-b]-thiophene-co-benzodithiophene
PV	-	Photovoltaics
SCLC	-	Space charge limited current
Se	-	Selenium
SRH	-	Shockley-Read-Hall
VB	-	Valence band

LIST OF SYMBOL

e	-	Elementary charge
h	-	Planck's constant
c	-	Velocity of light
λ	-	Wavelength of the incident photon
V_{oc}	-	Open circuit voltage
J_{sc}	-	Short circuit current density
R_s	-	Series area resistance
R_p	-	Parallel area resistance
E_g	-	Effective bandgap
N_c	-	Effective density of states in conduction band
N_v	-	Effective density of states in valence band
μ_n	-	Mobility of electron
μ_p	-	Mobility of hole
τ_n	-	Electron lifetime
τ_p	-	Hole lifetime
k	-	Boltzmann's constant
T	-	Absolute temperature
D_n	-	Diffusion coefficient of electron
D_p	-	Diffusion coefficient of hole
ϕ_1	-	Electron injection barrier
ϕ_2	-	Hole injection barrier
η	-	Overall cell efficiency
V_{bi}	-	Built-in potential
ε_0	-	Permittivity of free space
ε_r	-	Relative permittivity of the material
α	-	Absorption coefficient of the material
L_n	-	Diffusion length of electron

L_p	-	Diffusion length of hole
V_t	-	Thermal velocity
L	-	Active layer width
k_f	-	Geminate recombination rate
k_d	-	Separation rate of bound EHPs
a	-	Reaction radius
r_c	-	Onsager radius
E_c	-	Conduction band edge
E_v	-	Valence band edge
$n(x,V)$	-	Position and voltage dependent electron concentration
$p(x,V)$	-	Position and voltage dependent hole concentration
M	-	Escape probability
δ_n	-	Excess photo-generated electron concentration
δ_p	-	Excess photo-generated hole concentration
R	-	Recombination rate
E_{Fn}	-	Electron quasi-fermi level
E_{Fp}	-	Hole quasi-fermi level

CHAPTER 1: INTRODUCTION

1.1 Why need solar cell?

Solar energy is an important part in our life since the beginning of time. Increasingly, humans are trying to develop new techniques to make the best use of this vital resource and use it as a replacement of traditional energy sources like fossil fuels. In order to keep up with the growing energy consumption for an advanced living standard, the modern human civilization depends mostly on fossil fuels [1]. The pie chart in Fig. 1.1 shows the worldwide energy consumption in terms of primary energy sources. Figure 1.1 shows that about 87% of the total energy is produced from coal, natural gas and oil which are limited and cannot be replenished [2]. Another drawback of burning fossil fuels is the global warming. Therefore, the world will face a serious problem in future unless an alternative is found out. Solar energy is the best possible option to the scientists and researchers as the energy from sun is infinite. Moreover, it is considered as a clean energy source since it does not affect the environment or create a threat to Eco-systems the way oil and some other energy sources might. Furthermore, solar energy is inexpensive, free and abundantly available in most part of the world whereas the fossil fuels are expensive to retrieve from the earth and expensive to use [3].

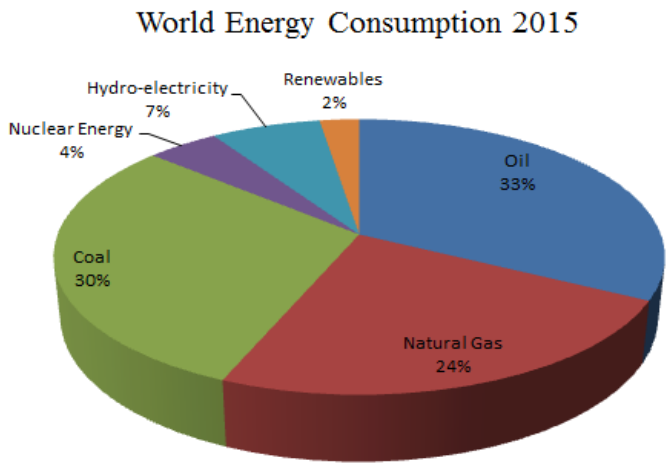

Figure 1.1 Energy consumption from primary energy sources in 2015 [2]

1.2 Background history and types

Alexandre Edmond Becquerel was the first who discovered the photovoltaic (PV) effect. In the year 1839 he observed the photo-electrochemical process when platinum (Pt) electrodes, covered with silver bromide (AgBr) or silver chloride (AgCl), were illuminated in aqueous solution. However, the first reports on photoconductivity were made by Smith and Adams in 1873 and 1876 respectively while working on selenium (Se). Anthracene ($C_{14}H_{10}$) was the first organic compound where photoconductivity was detected by Pochettino and Volmer in 1906 and 1913 respectively [4]. In the late 1950s and 1960s the potential use of organic materials as photoreceptors in imaging systems was recognized. In the early 1960s it was discovered that many common dyes, such as methylene blue, had semiconducting properties which were among the first organic materials to exhibit the PV effect. Although much progress has been made over the past few years organic PVs has not yet reached the market place unlike inorganic solar cells. In 1954, the first silicon inorganic solar cell was developed at Bell Laboratories by Chapin et al. This cell had an efficiency of 6%, which was later increased to 10% [5].

Basically, solar cells contain materials with semiconducting properties in which excitons are generated upon absorption of light energy and then separated by an internal electric field that induces a voltage and direct current when connected to a load. Generally, PV cells are of two kinds – organic and inorganic. Figure 1.2 shows the various types of PV cells. Almost 90% of the total PVs in the market are made of crystalline silicon because it is stable, it relies on established process technologies and in general it has proven to be reliable. The thin film technology based solar cells typically can achieve efficiencies of 7-13%. Although mass production of thin film solar cells is easier than crystalline-based modules, it requires a lot of space. Therefore, these modules are not suitable for residential application where space is an issue [6].

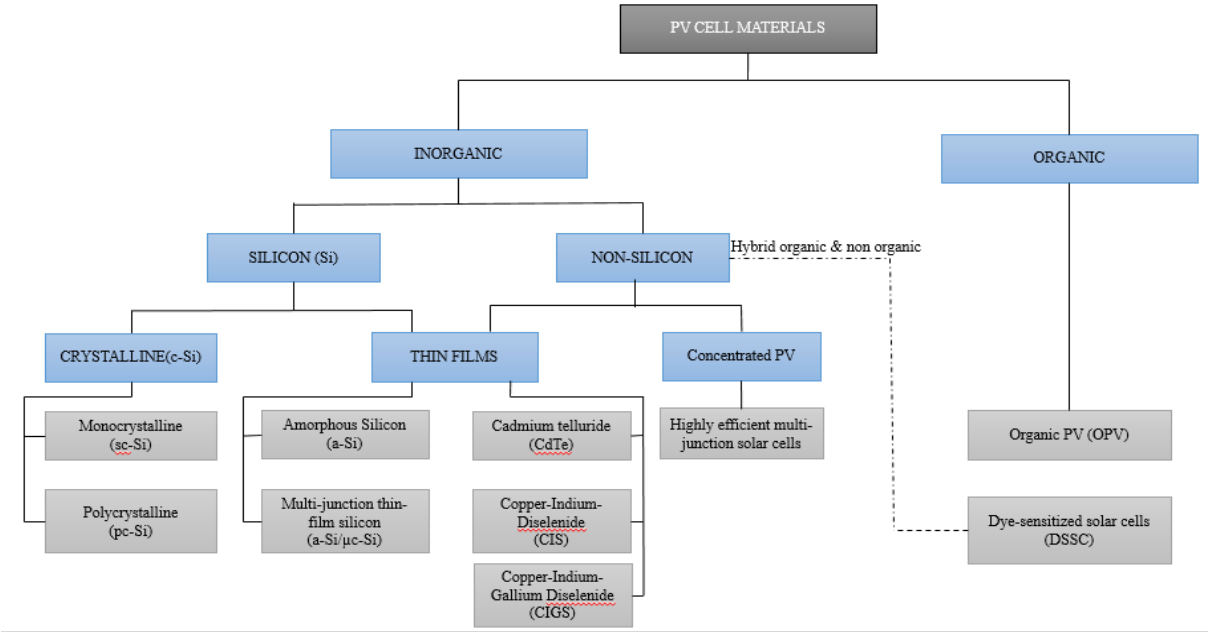

Figure 1.2 Classification of PV solar cells [7]

Another emerging and potential type of solar cell is the organic solar cell (OSC). They have low weight and very lower manufacturing cost compared to the conventional inorganic technologies. In addition, OPVs can be easily integrated into other products and most importantly has low environmental impact during manufacturing and operation [8]. The performance of the bulk heterojunction (BHJ) organic solar cells has been improved considerably during the last few years. Albeit BHJ models predict power conversion efficiencies in the range of about 10-15% but commercial BHJ-module with ~6% efficiency are feasible today [9]. Therefore, an extensive research on improving their performance is required to achieve the maximum efficiency.

1.3 Brief literature review and motivation

Bulk heterojunction (BHJ) polymer solar cells based on blends of conjugated polymers and fullerene derivatives (e.g., P3HT:PCBM blend) have made huge progress in research over the past decade due to their high conversion efficiency, solution-based easy fabrication, and abundant availability [10,11]. A clear knowledge and understanding the operating principles through accurate physics based modeling and optimization can make these cells

even more efficient, although currently they show a reasonable power conversion efficiency (almost 10%). A high binding energy of the bound electron-hole pairs (EHPs) due to low dielectric constant (ε_r) of organic materials reduces the number of photogenerated free carriers [12]. The photo generated electron and its twin hole (geminate pair) cannot immediately escape from their mutual columbic attraction. Therefore, it has to dissociate to create free charges. Not all the geminate pairs dissociate to free charges rather there is a dissociation probability *M*. Then the free carriers drift across the photoconductor layer (active layer) by the built-in electric field and some of the carriers are lost by deep trapping/recombination. At the optimum operating voltage, the built-in electric field is decreased which reduces the charge collection efficiency of the photogenerated carriers. Moreover, at the same time, the forward diode-like current (commonly known as the dark current) increases considerably. Both the photo and dark currents critically depend on the carrier transport properties of the blend (active layer) and cell structure. Thus the overall cell efficiency is mainly dominated by the photon absorption, dissociation efficiency of bound EHPs, charge collection efficiency and dark current.

Several groups have done research on the modeling of the current-voltage (J-V) characteristic of organic solar cells. For instance, Marsh et al. [13] offered a model where drift and diffusion charge transport has been neglected which limits its accuracy. Kumar et al. [14] proposed a model where the carrier generation and recombination processes are not taken into account. Again, a physics-based analytical model was given by Altazin et al. [15] assuming that the recombination rate is much smaller than the generation rate. Schilinsky et al. [16] modeled the BHJ solar cells without considering the initial recombination of photogenerated bound EHPs (i.e. dissociation efficiency of bound EHPs has been neglected). Several previous models [12,17] used Braun model based on Onsager theory, to compute the escape probability which does not agree well with the exact extension of Onsager theory [18]. The modified Braun's model is more accurate to estimate the escape probability since the BHJ OSCs operate within the valid field limit of the modified Braun's model.

Arnab et al. [19] proposed a model for the BHJ OSCs where an exponential photon absorption rate and actual solar spectrum are considered to measure the photocurrent densities at different voltages. Nevertheless, the model has used the common diode equation for dark current whose validity in BHJ solar cells has not yet been justified. And also the charge carrier concentrations at the contacts are not fixed in that model. Besides it ignored the contact effects. M.K. Alam et al. [20] proposed a physics-based analytical model for solar cells incorporating monomolecular recombination mechanism. In this model, a fixed carrier density is considered on both sides of the contacts. However, this model did not show any closed form dark current expression for the BHJ solar cells.

Therefore, an explicit physics-based model for the voltage-dependent photo and dark currents is highly desirable for enhancing the efficiency and optimizing the design. Thus, in this thesis, a complete model, including photo and dark current model for BHJ solar cells is proposed.

1.4 Research objective

The dark current versus voltage behavior has a significant effect on the overall current-voltage characteristics of the solar cell. Though the common diode equation has been used for the dark current, its validity in BHJ solar cells has not yet been justified [21]. Kumar et al. [14] proposed an analytical expression for the dark current considering carrier drift and diffusion across the active layer. Since there exists quasi fermi levels all over the active layer, the recombination current should be the dominant dark current mechanism in BHJ solar cells. Therefore, the objective of this thesis is to develop a comprehensive dark current model so that it can explain different effects (e.g. mobility and lifetime effects) on device performance. To achieve that goal, this research work is divided into several tasks:

- Firstly, to develop a physics-based mathematical model for the external voltage-dependent forward dark current by considering SRH recombination in the active layer and then compare the model calculations with the published experimental results on the dark current behavior.
- Secondly, to develop a model for photocurrent with proper boundary conditions and considering the contact effect. Then to find out the net external current of the

cells by summing up the dark and photocurrent, and compare it with the published experimental results.

- Finally, to compare the analytical model with the published experimental results in order to determine the carrier transport properties and, effects of charge dissociation and carrier transport properties on the cell efficiency. Also, to examine the effects of the contact properties, blend compositions, charge carrier transport properties (carrier mobility and lifetime), and cell design on the current-voltage characteristics.

1.5 Thesis outline

The thesis is outlined as follows:

Chapter 2 includes some fundamental knowledge necessary to understand the research work in this thesis. For instance, structure and properties of P3HT:PCBM blend and their working principles. Besides, the characteristics of BHJ organic solar cells i.e. J-V characteristics, incident photon to electron conversion are briefly discussed. Moreover, the existing J-V model for P3HT:PCBM is also outlined.

In Chapter 3, analytical voltage dependent dark current models are proposed based on different methods. These models are then investigated with three sets of experimental data on dark current. The best fitted model is then used for further calculation. Furthermore, the energy band diagram, recombination rate, carrier concentration in dark condition are also described.

Chapter 4 provides a voltage dependent photocurrent model. The best fitted dark current model from the previous chapter is chosen to calculate the net external current. Series and parallel resistances are also taken into account to get the net external photocurrent. Then, the model is fitted with the experimental data to verify its validity. The effects of various parameters such as thickness, carrier mobility, injection barrier, carrier lifetime on current-voltage characteristics are also shown.

Chapter 5 concludes the thesis summarizing the important outcomes of the thesis and mentioning further works for future research and improvement.

CHAPTER 2: BACKGROUND THEORY

2.1 Introduction

This chapter provides some background knowledges regarding organic solar cells so that this thesis work can be fully understood. The structure of the BHJ solar cells, material properties, operating principle, current-voltage (J-V) characteristics and existing J-V models are discussed here.

2.2 Structure of P3HT:PCBM blend organic solar cell

The bulk heterojunction (BHJ) organic solar cell (OSC) configuration is shown in Fig. 2.1, where poly (3-hexylthiophene) and [6,6]-phenyl-C_{61}-butyric acid methyl ester (P3HT:PCBM) are blended together to form the active layer in order to get high efficiency. P3HT and PCBM are used as donor and acceptor materials, respectively. The donor-acceptor blend is sandwiched between two electrodes with different work functions. The absorption coefficient depends on the weight ratio of P3HT:PCBM.

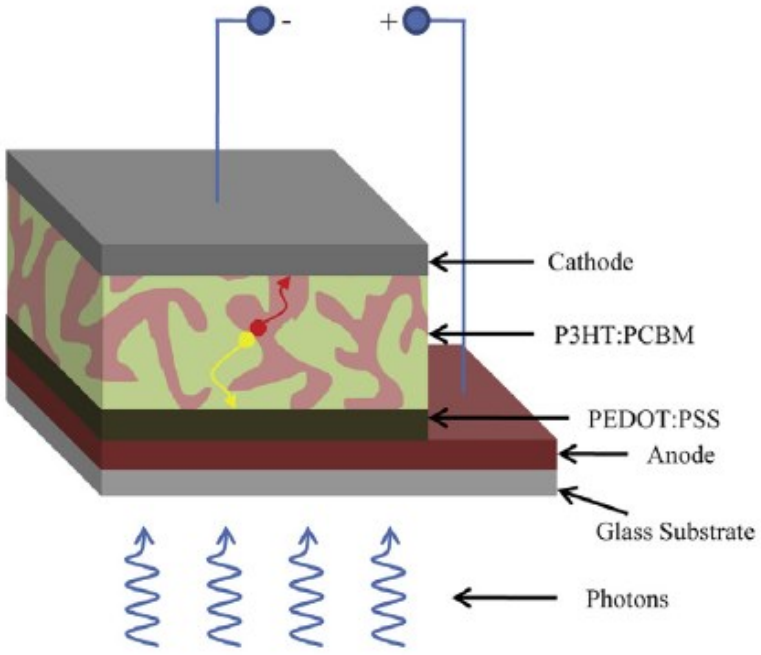

Figure 2.1 Configuration of P3HT:PCBM based BHJ OSC [20]

A transparent conductive polymer layer, poly(3,4-ethylenedioxythiophene):poly (styrenesulfonate) (PEDOT:PSS), is placed between the active layer and the anode to expedite the photogenerated holes to travel to the front contact. The anode (i.e. Indium Tin Oxide) forms an ohmic contact for easy movement of the generated carriers and also avoids unwanted absorption of the solar spectra. A schematic potential energy diagram of this structure (before the materials are brought into contact) is shown in Fig. 2.2.

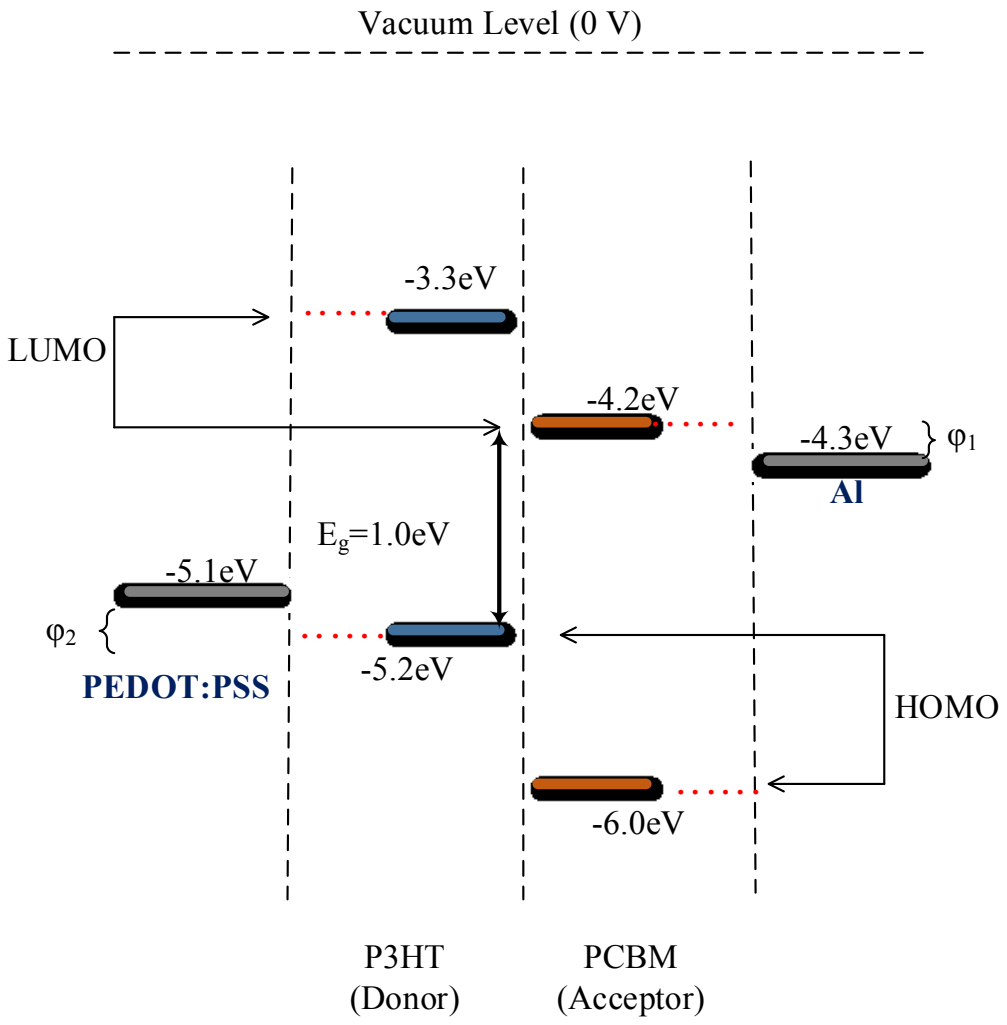

Figure 2.2 Potential energy diagram of BHJ OSC (before the contact) [20]

The dotted line indicates that there are many junctions in the active layer. For simplicity, only one junction is shown.

2.3 Properties of P3HT:PCBM blend

In recent years, conjugated polymers have drawn huge interest due to their solubility and electrical conductivity. Among all polymers, P3HT is widely used in the organic solar cell technology because of its large absorption coefficient (in the visible spectra in the order of 10^5 cm^{-1} [22]), low band gap energy, high carrier mobility. The chemical structures of P3HT and PCBM are shown in Fig. 2.3.

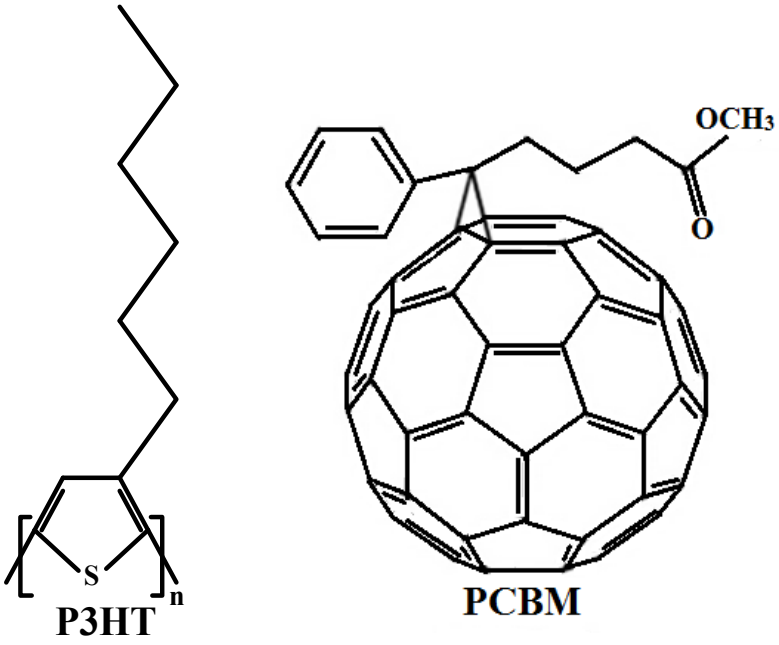

Figure 2.3 Chemical structure of P3HT and PCBM [scheme 1 of Ref. 23]

The PCBM is a fullerene derivative of the C_{60}. High electron affinity, good electron mobility and effective transport of charges have made fullerenes ubiquitous acceptors [24]. In the last decade, $PC_{60}BM$ and its corresponding C_{70} derivatives ($PC_{70}BM$) have been used as acceptors in organic solar cells (OSCs). Although $PC_{70}BM$ possesses strong absorption coefficient in the visible range, C_{70} is much more expensive due to its tedious purification process [25]. The electron affinity (X) of PCBM is ~4.2 eV, a bit larger than that of P3HT. Thus, electrons can be easily transferred from the lowest unoccupied molecular orbital of the donor (LUMO-D) to the LUMO of the acceptor (LUMO-A). The offset between the LUMO-D and the LUMO-A can be reduced by fine tuning of the band gap which in turn increases the open circuit voltage, V_{oc} [26]. There are several ways to tune the bandgap of

PCBM such as synthesizing bisadduct analogue of PCBM [26] and adding substituents on the phenyl ring or modifying the electronic band structure by electron irradiation [27]. Moreover, PCBM exhibits good solubility in organic solvent which makes it a suitable choice for BHJ solar cell.

Absorption coefficient of the blend can be improved by annealing at various temperatures and increasing the weight ratio of PCBM in the blend. Figure 2.4 represents the change in absorption coefficient of the blend with the weight ratio between P3HT and PCBM [28]. As we increase the weight ratio of PCBM in the blend, the absorption coefficient for the wavelength in between 425 and 700 decreases but below 425 nm it increases. When the PCBM weight percentage in the blend is increased beyond the 1:1 composition then a rapid decrease in the absorption coefficient is observed. The intermolecular packing structure of P3HT can be preserved if the weight ratio of PCBM is restricted below 1:1 composition [28].

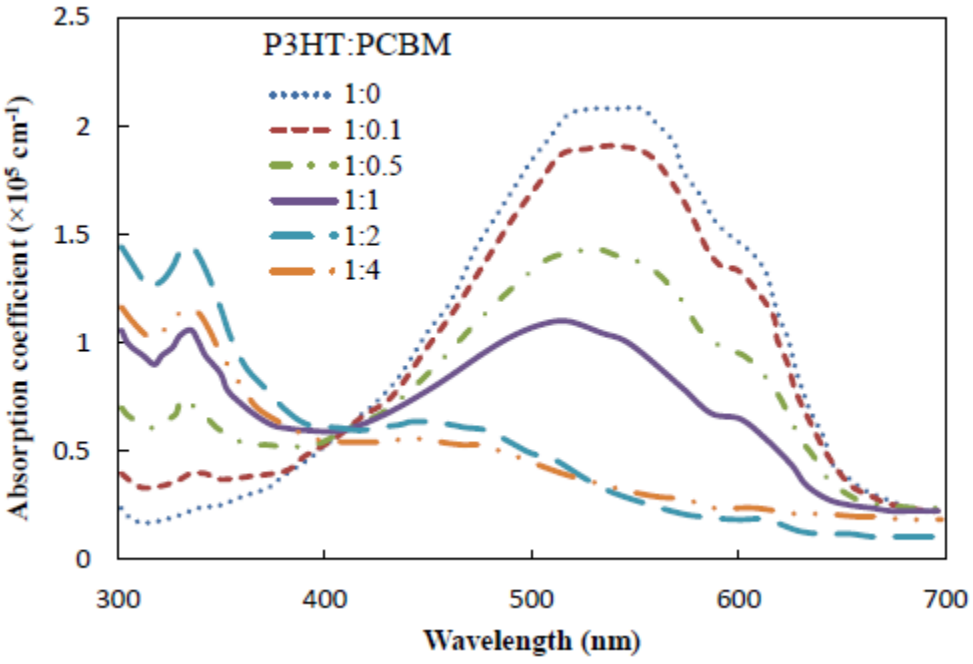

Figure 2.4 Absorption coefficient vs different weight ratio between P3HT and PCBM [28]

Annealing is a way of improving the efficiency of polymer photovoltaic cells. Optical properties and microphase separation of the blend can be changed by this method. Fig. 2.5

depicts the absorption spectra of the PSC devices based on P3HT:$PC_{61}BM$ blend treated at three different temperature. It has been found that if the annealing temperature is increased from 130°C to 150°C the short-circuit current (J_{sc}) is increased from 11.56 mA/cm^2 to 12.78 mA/cm^2 [29]. It is because the higher the temperature is the more the crystallinity of PCBM in blend is enhanced. However, the highest PCE is obtained at 170°C which is 4.55% though the J_{sc} is decreased. The reason behind this is $PC_{61}BM$ clusters length is expanded with the temperature. Higher performance is achieved if $PC_{71}BM$ is used instead of $PC_{61}BM$ in the blend [29].

Table 2.1 shows the charge carrier properties of the fullerene-polymer organic solar cell. The data given in the table are found experimentally by different researchers. In polymer-fullerene based organic solar cells usually the mobility of electrons is a bit higher than the holes. Some researchers did not specify the electron and hole transport properties (mobility and lifetimes) separately rather they used a common value for all carriers. The parameters used to simulate the models that will be discussed in the next two consecutive chapters, have a good agreement with the mentioned range.

Table 2.1 Charge carrier dynamics for P3HT:$PC_{61}BM$ blend in BHJ organic solar cells.

Carrier mobility (cm^2/V-s)	**Carrier lifetime (sec)**	**Blend ratio (P3HT:$PC_{61}BM$)**	**Reference**
9.4×10^{-4}	1×10^{-5}	1:0.8	30
2×10^{-3}	$\sim 3\text{-}1\times10^{-4}$	1:0.75	31
5×10^{-4}	not mentioned	1:0.8	32
3×10^{-3} (electron) 2×10^{-4} (hole)	0.2×10^{-6} (electron) 1×10^{-6} (hole)	1:1	33
$\sim1\times10^{-3}$ (electron) $\sim1\times10^{-4}$ (hole)	$\sim50\times10^{-6}$ (bound pair lifetime)	1:1	34

Fig. 2.5 shows the absorption spectra of the P3HT: PCBM blend with the change of temperature. Absorption spectra does not change much with the increase of temperature.

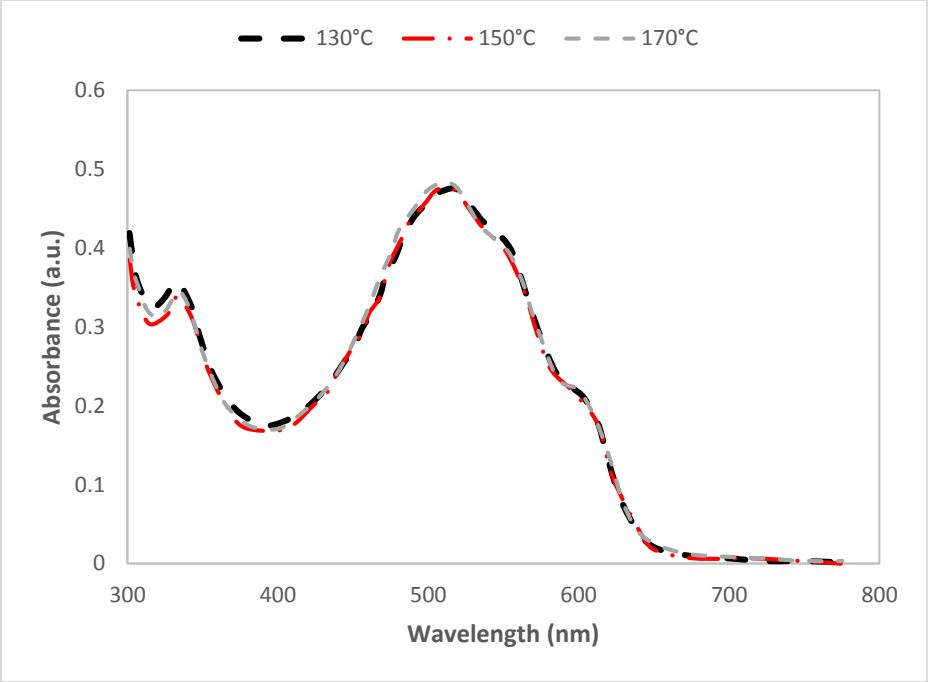

Figure 2.5 Absorption spectra of the P3HT:$PC_{61}BM$ blend for three different temperatures [Fig 6 of Ref. 29]

2.4 Working principles of organic solar cells

Solar cells convert the optical energy into the electrical energy upon absorption of light particles or photons. This conversion process is done through several steps. These steps are as follows.

2.4.1 Photon absorption and exciton generation

When photons are incident on the P3HT:PCBM solar cell they will be absorbed in the blend. However, instead of generating free carriers bounded electron-hole pairs will be created because of the low dielectric constant of organic material [35,36]. This bounded electron-hole pair is called an exciton, with a binding energy of 0.1-1.4 eV [31], very high value compared to the inorganic semiconductors. That is why, in inorganic materials electron-hole pair can be dissociated easily by absorbing thermal energy. The photon absorption also depends on the absorption coefficient of the active layer (10^5 cm^{-1} for organic materials [37]) and its thickness. Although OSCs have thickness limitations, a few hundreds of nanometers of the absorber layer is thick enough to absorb sufficient amount

of light [38]. Fig. 2.6 shows the sun spectrum at AM 1.5 [39]. It has been observed that almost 77% of the light spectrum is absorbed when the LUMO-HOMO difference is 1.1 eV [40]. The absorption efficiency can be improved if small band gap materials are used.

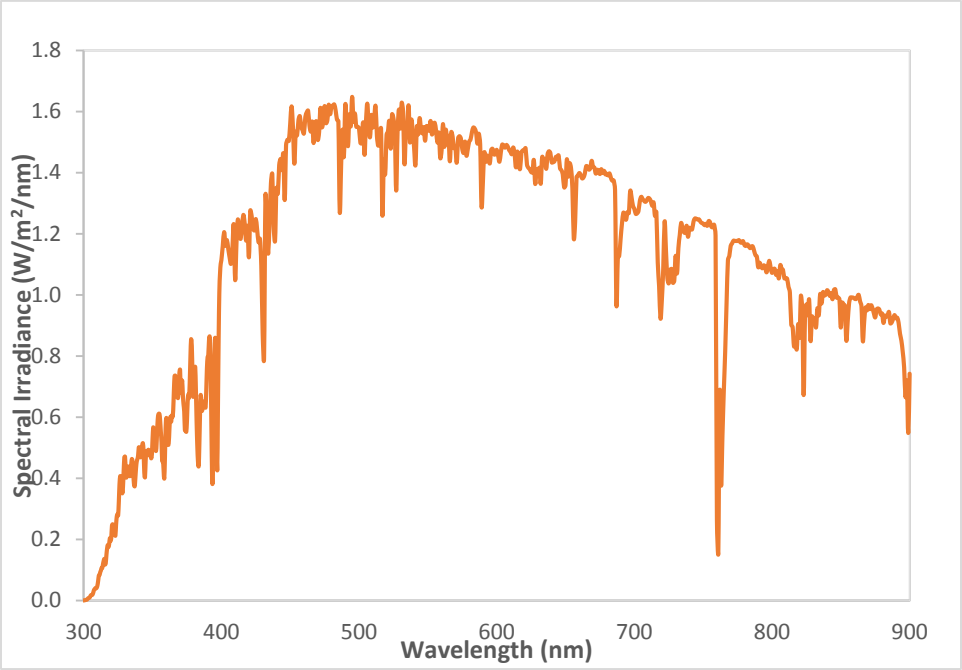

Figure 2.6 Solar spectrums at AM1.5 [39]

2.4.2 Exciton diffusion and dissociation

The next step is to separate the bound electron-hole pairs so that they can lead to electricity generation. This is done by introducing a secondary organic material in the active which has an energetically lower lying LUMO-level (as shown in Fig. 2.7). If an exciton is generated in donor material, it drifts towards the heterojunction and the electron then can easily transfer from the exciton to LUMO of acceptor as the potential difference between the donor HOMO and acceptor LUMO is lower than the energy of the exciton, while the hole remains in the donor HOMO. For this reason, the material with the highest LUMO is called the electron donor while the other is called the electron acceptor. After the dissociation at the heterojunction, electron-hole pair forms a charge pair called a geminate pair, which are still bounded by the coulombic attraction. Hence, a strong internal field is required to separate them.

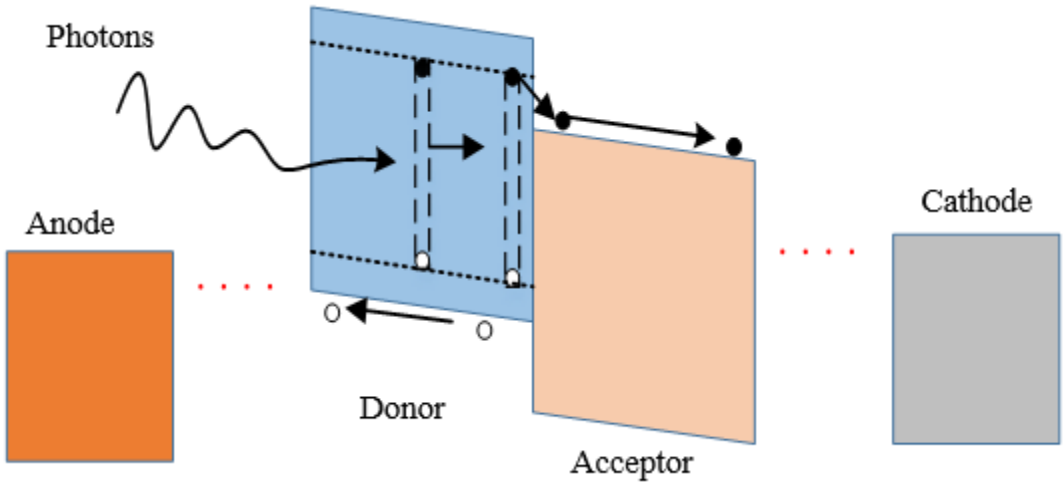

Figure 2.7 The process of photon absorption to photocurrent generation in P3HT:PCBM blend

The average distance that an exciton travels before recombination is the diffusion length. If an exciton generates at a distance from the heterojunction longer than its diffusion length then it will recombine before it gets dissociated. Hence, the active layer has to be kept thin to increase the dissociation efficiency. Again, if the length of the absorber layer is decreased then there will be lower absorption. Therefore, an optimum thickness is selected to achieve the highest efficiency.

2.4.3 Charge carrier transport

After the dissociation process, the charge pairs have to travel to electrodes for collection before they recombine. Drift and diffusion currents are the main driving forces for the charge transport. The drift current results from the carrier movement along the potential gradient within the solar cell, whereas the diffusion of carriers along the concentration gradient generates diffusion current. The potential gradient is the difference between the work functions of the two electrodes. Usually, anode with higher work function and cathode with lower work function are selected and this difference creates a built-in electric field that determines the open circuit voltage (V_{oc}) of the cell. An external bias will modify the internal electric field and the carriers will move along the resultant internal electric field

towards the respective electrodes for collection. Another charge transport mechanism is the diffusion. The concentration of electrons and holes are actually higher around the heterojunction because geminate pairs are generated around the heterojunction. For this reason, carriers will diffuse along the concentration gradient away from the heterojunction. The diffusion current mostly dominates when the applied external bias will almost nullify the internal electric field.

The carrier transport is limited by the mobility in the active layer. Since hole and electron mobilities are lower in organic materials, the active layer thickness should be kept as small as possible to allow the carriers to reach the electrodes before they recombine.

2.4.4 Charge collection at electrodes

When the charge carriers reach to their respective electrodes, they are extracted from the active layer. To obtain the highest efficiency in charge collection, the potential barriers at the active layer/electrode interfaces have to be minimized. Therefore, the anode and cathode are selected very carefully so that the anode work function matches the donor HOMO and the cathode work function matches the acceptor LUMO. This type of contact is called the ohmic contacts.

Usually, indium tin oxide (ITO) is used as an anode material as it has a very high work function of about 4.7 eV [38] and a good match with the HOMO of P3HT [41]. Instead of ITO, high work function metals (e.g. Au (5.1 eV)) can also be used as an anode contact [42]. For cathode contact, low work function metals such as Al (4.2 eV) are mainly used. There are several ways to achieve the work function matching, e.g. changing absorber materials, and inserting interlayers between the electrodes and the active layer. Besides,

increasing the roughness or interface area of the electrodes can improve the charge collection efficiency [43,44].

2.5 Characterization of OSCs

2.5.1 Current-voltage characteristics

Accurate measurement and characterization of OSCs are typically done under 1000 W/m^2 light of AM 1.5 solar spectrums [45]. The J-V curve can be explained by the Shockley solar cell equation,

$$J(V) = J_{dark}(V) - J_{ph}(V) + \frac{V - JR_s}{R_p} \tag{2.1}$$

where V is the applied bias, J is the net external current density, J_{dark} is the dark current density, J_{ph} is the photocurrent density and R_s, R_p are the series and parallel area resistances respectively. The J-V curve represents a number of parameters which are used to evaluate the performance of a solar cell such as open circuit voltage (V_{oc}), short circuit current density (J_{sc}), fill factor (FF), power conversion efficiency (PCE), series resistance (R_s) and parallel resistance (R_p). Fig. 2.8(a) shows the equivalent circuit model of a practical solar cell and 2.8(b) represents the J-V characteristics of a solar cell. The basic parameters are described below.

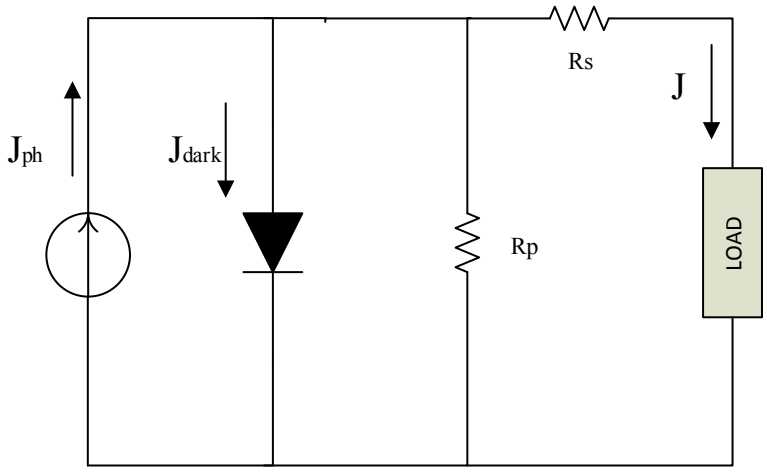

(a)

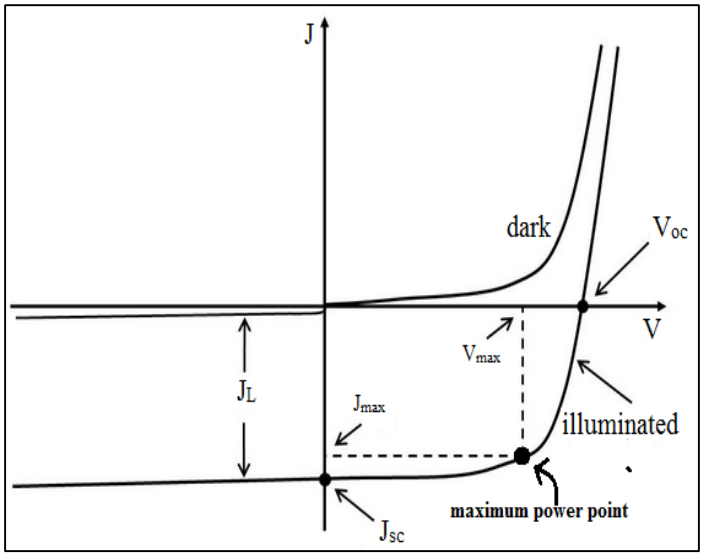

(b)

Figure 2.8 (a) Equivalent circuit model of practical solar cell. (b) J-V curve of a typical solar cell showing both dark and illuminated curves separately [Fig. 2 of Ref. 46].

2.5.1.1 Short circuit current density (J_{sc})

The short-circuit current is the current at which the external applied voltage is 0 i.e. the output terminal is in short circuit condition. J_{sc} denotes the net current density in the external circuit at the short-circuit condition. Fig. 2.8(b) shows the J_{sc} in the J-V curve. In ideal condition, short-circuit current is equal to the photocurrent.

2.5.1.2 Open circuit voltage (V_{oc})

The open circuit voltage is the maximum voltage available from a solar cell when the terminal is open. V_{oc} mainly depends on the work function of metal contacts. If the contact is Ohmic, V_{oc} is then dependent on the HOMO-LUMO difference between the donor and acceptor [35]. V_{oc} can be calculated by setting the net current equal to zero in the solar cell Eq. 2.1,

$$V_{oc} = nV_t \ln\left(\frac{J_{ph}}{J_o} + 1\right), \text{ when } J_{dark} = J_o\left(\exp\left(\frac{V}{nV_t}\right) - 1\right) \tag{2.2}$$

where n is the ideality factor and J_o is the reverse saturation current density, $V_t = kT/e$ is the thermal voltage.

2.5.1.3 Fill factor (*FF*)

Fill factor explains the solar cell performance and can be calculated from the J-V curve as follows,

$$FF = \frac{J_{\max} V_{\max}}{J_{sc} V_{oc}} \tag{2.3}$$

where $J_{\max}$ and $V_{\max}$ are the current density and voltage for maximum output power respectively. As shown in the equation above, FF is the ratio of the maximum output power to the maximum attainable output power. Graphically it is a measure of 'squareness' of the solar cell and also defines the area of the largest rectangle that fits in the J-V curve.

2.5.1.4 Power conversion efficiency (PCE)

PCE is the ratio of maximum output power to the input power and can be calculated by the following expression,

$$PCE = \frac{P_{\max}}{P_{in}} = \frac{V_{oc} J_{sc} FF}{P_{in}} \tag{2.4}$$

where P_{in} is the input optical power density.

2.5.1.5 Series resistance (R_s)

Series resistance arises due to the charge carrier movement in the semiconductor materials, contact resistance between semiconductor and electrodes and the resistance of the electrode materials. High value of series resistance can reduce J_{sc} which in turn lower the fill factor of the solar cell. R_s can be defined as the inverse of the slope of J-V curve at the V_{oc} point.

2.5.1.6 Parallel resistance (R_p)

Shunt or parallel resistance can cause significant power loss in the solar cell. Due to the manufacturing defects, alternate path may be created for the light-generated carriers to move and eventually recombine. For low parallel resistance, these carriers may take these alternate path which results in low photocurrent flow through the external circuit.

2.5.2 Incident photon to electron conversion efficiency (IPCE)

To characterize a solar cell fully J-V characteristics are not quite adequate as they lack information about the optical factors. For this reason, the measure of incident photon to electron conversion efficiency is needed. IPCE is equivalent to external quantum efficiency (EQE). It is the ratio of the number of charge carriers collected by the electrodes to the number of photons of a given energy incident on the solar cell from outside. IPCE is highly dependent on the absorption curve of the active layer.

2.5.3 Existing J-V model for P3HT:PCBM blend of BHJ OSCs

The photocurrent for an ideal solar cell does not depend on the external voltage and is given by the following equation,

$$J_{ph} = egL \tag{2.5}$$

where, g is the generation rate and L is the active layer length. The recombination rate is neglected in the ideal solar cell assuming that the carrier lifetime is greater than the transit time.

Sokel and Hughes et al. [47] proposed a voltage dependent photocurrent model in which diffusion current is considered and the photocurrent is determined by the equation below,

$$J_{ph}(V) = egL\left(\frac{\exp\left(\frac{eV}{kT}\right)+1}{\exp\left(\frac{eV}{kT}\right)-1} - \frac{2kT}{eV}\right) \tag{2.6}$$

However, their model is based on an empirical expression. Besides, the J-V curve of this model cannot explain clearly the exact effect of various important parameters.

The performance of BHJ solar cells mostly depends on the dissociation efficiency of the blend layer. Therefore, Deibel et al. [48] suggested a model where carrier generation is estimated based on Braun model. The field dependent generation rate is given by

$$g'(T,F) = g \times P(T,F) \tag{2.7}$$

where, P is the electric field dependent dissociation efficiency and is given by the following equation,

$$P(T,F)=\frac{k_d(F)}{k_d(F)+k_f} \tag{2.8}$$

and

$$k_d(F)=\frac{3e\mu}{4\pi\varepsilon a^3}\exp\left(-\frac{E_b}{kT}\right)\frac{J_1\left(2\sqrt{-2b}\right)}{\sqrt{-2b}} \tag{2.9}$$

$$b=\frac{e^3F}{8\pi\varepsilon(kT)^2} \tag{2.10}$$

where, μ is the sum of the electron and hole mobility, a is the initial polaron-pair radius, F is the electric field, ε is the effective dielectric constant, E_b is the coulombic binding energy and k_f is the geminate recombination rate. However, the dissociation efficiency, which has been calculated by the Braun model, is based on the Onsager theory. Later, Wojcik and Tachiya [18] showed that the difference between Braun model and the exact extension of Onsager theory is significant and cannot be ignored.

Schilinsky et al. [16] proposed a photocurrent model based on the average mean carrier distance. According to the model, the photo generated current density can be written as,

$$J_{ph}(V)=\begin{cases}-|J_{sc}| \Rightarrow if\ \dfrac{\mu\tau(-V+V_{bi})}{L}>L\\ |J_{sc}| \Rightarrow if\ \dfrac{\mu\tau(-V-V_{bi})}{L}>L\\ |J_{sc}|\times\dfrac{\mu\tau(-V+V_{bi})}{L^2}else\end{cases} \quad \text{where } V_{bi} \text{ is the built-in potential} \tag{2.11}$$

However, in the above equation direct carrier recombination is not taken into account. Besides, an internal quantum efficiency of 100% is assumed while estimating the J_{sc}, whereas a lot of carriers are lost due to geminate recombination.

CHAPTER 3: ANALYTICAL DARK CURRENT MODEL

3.1 Introduction

In this chapter, a physics based analytical dark current model and its mechanism will be discussed. In organic donor-acceptor (DA) solar cells, the current that flows in the absence of light illumination is called the dark current. Dark current is a very important parameter in OSCs as this current limits the performance of a solar cell. In many previous works, Shockley diode equation was used to model the dark current in donor-acceptor organic bulk heterojunction solar cells. The Shockley diode equation is good for p-n abrupt diodes. The BHJ structure is not exactly a p-n diode. Therefore, the models based on Shockley equation cannot properly describe the processes responsible for dark current. For this reason, an analytical model for dark current analysis is necessary to describe all the unexplained matters.

The dominating loss factor in BHJ organic solar cells is one of the most debated topics in recent time. In early BHJ, the initial geminate recombination was the dominant loss mechanism [12]. The dissociation efficiency has been improved in some recent blends and becomes close to unity. For example, cells made of a blend of the conjugated polymer poly[N-9”-hepta-decanyl-2,7-carbazole-alt-5,5-(4’,7’-di-2-thienyl-2’,1’,3’-benzothiadiazole)] (PCDTBT) with the soluble fullerene derivative (PCBM) show near to unity dissociation efficiency [49]. However, their cell efficiency strongly depends on the charge collection efficiency due to trapping/recombination of free carriers. Traditionally, bimolecular recombination processes in organic solar cells have been discussed extensively in the scientific literature and Shockley-Read-Hall (SRH) interface states at the bulk heterojunction has been considered, but largely discarded. Recently, however, Street et al. [21] concluded that recombination of mobile carriers at SRH-type interface states at or near the buried heterojunction is the dominant recombination mechanism. Shuttle et al [50] showed that the bimolecular recombination coefficient depends on the charge carrier concentration in a way that the recombination coefficient becomes equivalent to the SRH-type trap-assisted recombination. Moreover, Mandoc et al. [51] showed that, for 1 sun

intensity or less, the SRH-type recombination dominates over the bimolecular recombination. Therefore, for simplicity, the trap-assisted (first order) monomolecular recombination is considered in this thesis.

Since there exist quasi fermi levels all over the active layer if an external voltage is applied, the recombination current should be the dominant dark current mechanism over drift and diffusion currents in the OSCs. This chapter combines selected material from my published journal paper.[1]

3.2 Theoretical dark current model

The active layer or blend layer is contacted by two metals: one of high work function, ϕ_a (anode) and the other one of low work function, ϕ_c (cathode). The work function difference is called the built-in potential,

$$eV_{bi} = \phi_a - \phi_c = E_g - \phi_1 - \phi_2, \tag{3.1}$$

Due to this work function difference of the metals, the bands are tilted. When the applied bias is zero, the fermi-levels of the both sides are aligned together. The voltage applied between the contacts modifies the tilt of the band which results in the change in electric field across the active layer. When the blend layer is contacted by the metals, the system comes to equilibrium within a very short time and then the fermi levels of the both sides are homogeneous (i.e. are fixed at the same energy level). Fig. 3.1 represents the energy band diagram of a BHJ organic solar cell at thermal equilibrium. However, once there exists the external voltage in the system, this voltage creates a separation of fermi levels which we call quasi-fermi levels that reduces the tilt of the bands and the electric field of the layer.

[1] Saleheen, M., Arnab, S. M., & Kabir, M. Z. (2016). Analytical Model for Voltage-Dependent Photo and Dark Currents in Bulk Heterojunction Organic Solar Cells. *Energies*, *9*(6), 412.

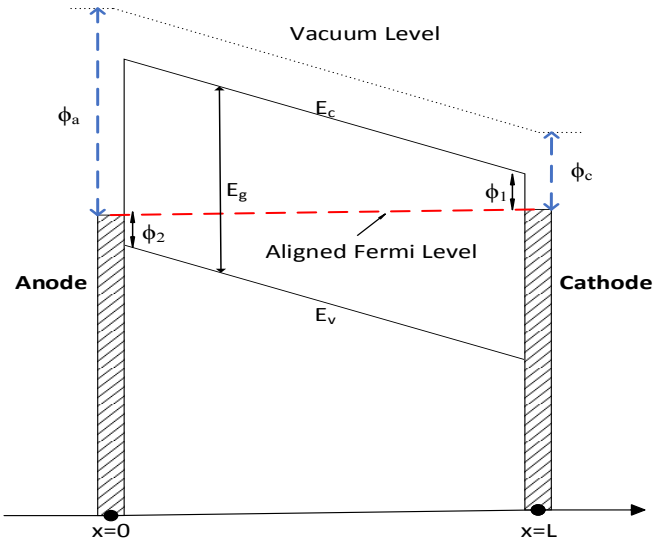

Figure 3.1 A typical energy band diagram of a BHJ solar cell under zero applied bias (*V=0*). Here *x* is the distance from the anode (radiation-receiving electrode).

The free electrons in the active layer travel through the acceptor towards the back contact whereas the holes remain in the donor and travel towards the radiation-receiving electrode (top contact). The free carriers move both by the drift and diffusion. The built-in electric field in the active layer assists the drift process. Hernandez-Garcia et al. [52] showed that the electric field is almost uniform across the active layer if the layer thickness is in the range of few hundreds nm or less. In fact, the optimum active layer thickness for the BHJ photovoltaics is 70-200 nm [49,53]. Therefore, the electric field F is considered uniform across the active layer. The drift mobility (μ) and carrier lifetime (τ) of holes and electrons are also considered uniform to allow the problem to be analytically tractable [54].

The diode equation that is commonly used for the dark current is, [55,56]

$$J_d(V) = J_o \exp\left(\frac{V - JR_s}{nV_t}\right) \tag{3.2}$$

where J_o is the reverse saturation current density, R_s is the series area resistance, V_t is the thermal voltage and n is the ideality factor. In standard p-n junction theory, $n = 2$ is identified as a value for junction recombination and $n = 1$ represents the neutral region recombination. In the dark condition, recombination is the dominant mechanism for

generating current. It has been reported that for polymer-fullerene organic solar cells, ideality factors ranges from 1.3-2.0. R. A. Street et al. [21] suggested that the ideality factor, $n \approx 1.65$, T. Kirchartz et al. [57] shows that $n = 1.6$, L. J. A. Koster et al. [58] mentioned that at room temperature ideality factor, n typically amounts to 1.4.

Though the common diode equation has been used for the dark current, its validity in BHJ solar cells has not yet been justified. In fact, the dark current behavior significantly varies among the experimental results [59,60]. In this thesis, the expression of dark current is derived solving physical equations and via adopting three slightly different methods. These methods are described below.

3.2.1 Adapting the assumption of K. Taretto [61]

According to Fig. 3.1 the equilibrium electron concentration in the blend layer is given by [61]

$$n_0(x) = n_0 \exp\left(-\frac{F_0}{V_t}x\right), \tag{3.3}$$

where, F_0 and n_0 are the thermal equilibrium electric field and thermal equilibrium electron concentration (at x=0) respectively and can be defined as follows.

$$F_0 = \frac{-V_{bi}}{L} \tag{3.4}$$

$$n_0 = N_c \exp\left(-\frac{E_g - \phi_2}{eV_t}\right) \tag{3.5}$$

If the effective density of states for both the conduction and valence bands are considered to be same i.e. ($N_c = N_v$) then the equation (3.5) will become,

$$n_0 = n_i \exp\left(-\frac{E_g - 2\phi_2}{2eV_t}\right) \tag{3.6}$$

Now, to calculate the carrier concentration, continuity equation needs to be solved. The continuity equation for electron in the blend layer can be written as

$$-\frac{1}{e}\frac{d}{dx}J_n(x) = G_n(x) - R_n(x) \tag{3.7}$$

where, G_n and R_n are the generation and recombination rate respectively. $R_n(x)$ and $J_n(x)$ can be defined as

$$R_n = \frac{n(x) - n_0(x)}{\tau_n} \tag{3.8}$$

$$J_n(x) = e\mu_n n(x)F + eD_n \frac{dn(x)}{dx} \tag{3.9}$$

where, τ_n is the electron lifetime. $G_n = 0$ for dark condition.

If the expression of Eq. (3.9) is used in Eq. (3.7) then it becomes

$$-\mu_n F \frac{dn(x)}{dx} - D_n \frac{d^2 n(x)}{dx^2} = -\frac{n(x) - n_0(x)}{\tau_n}$$

$$\Rightarrow \frac{d^2 n(x)}{dx^2} + \frac{F}{V_t}\frac{dn(x)}{dx} - \frac{n(x)}{L_n{}^2} = -\frac{n_0(x)}{L_n{}^2}, \text{ where } L_n = \sqrt{D_n \tau_n} \tag{3.10}$$

Therefore, the solution of Eq. (3.10) would be

$$n(x,V) = A_1 \exp(m_1 x) + A_2 \exp(m_2 x) + \frac{n_0}{C^*}\exp\left(-\frac{F_0}{V_t}x\right) \tag{3.11}$$

where $C^* = 1 + F_0\left(\frac{L_n}{V_t}\right)^2 (F - F_0)$, $F = \frac{V - V_{bi}}{L}$ and $m_{1,2} = -\frac{F}{2V_t} \pm \sqrt{\left(\frac{F}{2V_t}\right)^2 + \frac{1}{L_n{}^2}}$

The boundary conditions for the electrons are:

$$n(0) = n_i \exp\left(-\frac{E_g - 2\phi_2}{2eV_t}\right) \tag{3.12}$$

$$n\left(\frac{L}{2}\right) = n_0\left(\frac{L}{2}\right)\exp\left(\frac{V}{2V_t}\right) = n_i \exp\left(\frac{\phi_2 - \phi_1}{2eV_t}\right)\exp\left(\frac{V}{2V_t}\right) \tag{3.13}$$

The second boundary condition will be valid if the device is symmetric [61] (i.e. if the injection barriers in both sides of the active layer are equal ($\phi_1 = \phi_2$)).

The constants A_1 and A_2 can be calculated applying these boundary conditions in Eq. (3.11).

$$A_1 = \frac{n_i\left[\exp\left(m_2\frac{L}{2}-\frac{E_g-2\phi_2}{2eV_t}\right)\left(1-\frac{1}{C^*}\right)-\exp\left(\frac{\phi_2-\phi_1}{2eV_t}\right)\left\{\exp\left(\frac{V}{2V_t}\right)-\frac{1}{C^*}\right\}\right]}{\exp\left(m_2\frac{L}{2}\right)-\exp\left(m_1\frac{L}{2}\right)} \tag{3.14}$$

$$A_2 = \frac{n_i\left[\exp\left(m_1\frac{L}{2}-\frac{E_g-2\phi_2}{2eV_t}\right)\left(1-\frac{1}{C^*}\right)-\exp\left(\frac{\phi_2-\phi_1}{2eV_t}\right)\left\{\exp\left(\frac{V}{2V_t}\right)-\frac{1}{C^*}\right\}\right]}{\exp\left(m_1\frac{L}{2}\right)-\exp\left(m_2\frac{L}{2}\right)} \tag{3.15}$$

Since half of the length of the entire active layer region is p-type and the rest of it is n-type, the recombination current due to minority carrier electron in the first half,

$$J_{rn} = e\int_0^{L/2}\frac{n(x)-n_0(x)}{\tau_n}dx$$

$$\text{or, } J_{rn} = \frac{e}{\tau_n}\left[\frac{A_1}{m_1}\left\{\exp\left(m_1\frac{L}{2}\right)-1\right\}+\frac{A_2}{m_2}\left\{\exp\left(m_2\frac{L}{2}\right)-1\right\}-\frac{V_t}{F_0}n_0\left(\frac{1}{C^*}-1\right)\left\{\exp\left(\frac{V_{bi}}{2V_t}\right)-1\right\}\right] \tag{3.16}$$

Similarly, solving the continuity equation for holes the following equation can be derived

$$p(x,V) = B_1\exp(k_1x)+B_2\exp(k_2x)+\frac{p_0}{D^*}\exp\left[-\frac{F_0}{V_t}(L-x)\right], \tag{3.17}$$

where $k_{1,2} = \frac{F}{2V_t}\pm\sqrt{\left(\frac{F}{2V_t}\right)^2+\frac{1}{{L_p}^2}}$, $D^* = 1+F_0\left(\frac{L_p}{V_t}\right)^2(F-F_0)$

and $p_0 = n_i\exp\left(-\frac{E_g-2\phi_1}{2eV_t}\right)$

The boundary conditions for holes are:

$$p(L) = n_i\exp\left(-\frac{E_g-2\phi_1}{2eV_t}\right) \tag{3.18}$$

$$p\left(\frac{L}{2}\right) = p_0\left(\frac{L}{2}\right)\exp\left(\frac{V}{2V_t}\right) = n_i\exp\left(\frac{\phi_1-\phi_2}{2eV_t}\right)\exp\left(\frac{V}{2V_t}\right) \tag{3.19}$$

Applying boundary conditions in Eq. (3.17) we get the constants B_1 and B_2

$$B_1 = \frac{n_i\left[\exp\left(-\frac{E_g-2\phi_1}{2eV_t}-k_2\frac{L}{2}\right)\left(1-\frac{1}{D^*}\right)-\exp\left(\frac{\phi_1-\phi_2}{2eV_t}\right)\left\{\exp\left(\frac{V}{2V_t}\right)-\frac{1}{D^*}\right\}\right]}{\exp\left(k_1\frac{L}{2}\right)\left[\exp\left\{(k_1-k_2)\frac{L}{2}\right\}-1\right]} \tag{3.20}$$

$$B_2 = \frac{n_i\left[\exp\left(-\frac{E_g-2\phi_1}{2eV_t}-k_1\frac{L}{2}\right)\left(1-\frac{1}{D^*}\right)-\exp\left(\frac{\phi_1-\phi_2}{2eV_t}\right)\left\{\exp\left(\frac{V}{2V_t}\right)-\frac{1}{D^*}\right\}\right]}{\exp\left(k_2\frac{L}{2}\right)\left[\exp\left\{(k_2-k_1)\frac{L}{2}\right\}-1\right]} \tag{3.21}$$

Hence, recombination current due to hole will be,

$$J_{rp} = e\int_{L/2}^{L}\frac{p(x)-p_0(x)}{\tau_p}dx$$

or,

$$J_{rp} = \frac{e}{\tau_p}\left[\frac{B_1}{k_1}\left\{\exp(k_1L)-\exp\left(k_1\frac{L}{2}\right)\right\}+\frac{B_2}{k_2}\left\{\exp(k_2L)-\exp\left(k_2\frac{L}{2}\right)\right\}+\frac{V_t}{F_0}p_0\left(\frac{1}{D^*}-1\right)\left\{1-\exp\left(\frac{V_{bi}}{2V_t}\right)\right\}\right] \tag{3.22}$$

Therefore, the total current would be the sum of Eq. (3.16) and Eq. (3.22)

$$J_{dark} = J_{rn} + J_{rp} \tag{3.23}$$

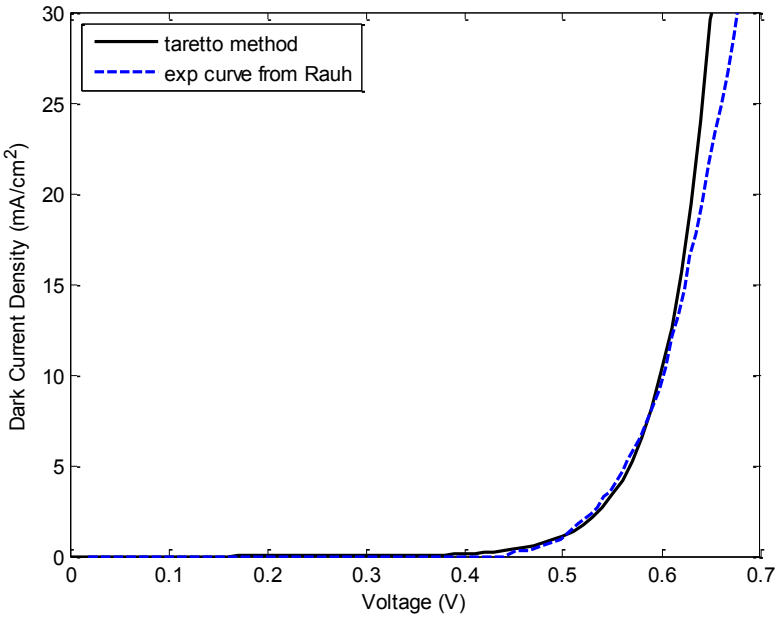

Figure 3.2 Experimental curve from Rauh et al. [59] (blue dashed line) and derived dark current (black solid line) model from Taretto with respect to applied bias.

Figure 3.2 above represents the dark current density (J) as a function of voltage (V). The black solid line represents the simulation result (equation 3.23) and the blue dashed line is the experimental curve taken from Rauh et al. [59]. The parameters taken to simulate the model are shown in Table 3.1. The lifetimes for both electron and hole are kept constant at 6 µs. It appears that the model fits well with the experimental curve initially when the voltage is low. However, a significant mismatch is observed when the voltage is increased.

3.2.2 Fixed carrier concentration at the boundaries

Continuity equation for electron concentrations is

$$\frac{1}{e}\frac{dJ_n(x)}{dx} + G_n - R_n = 0, \tag{3.24}$$

where G_n is the electron generation rate, R_n is the recombination rate ($= r_m n(x) = \frac{n(x)}{\tau_n}$; where r_m is the monomolecular recombination coefficient), $J_n(x)$ is the electron current density

When there is no illumination then no excess carrier will be generated (i.e. $G=0$). $J_n(x)$ can be expressed as:

$$J_n(x) = q\mu_n n(x)F + qD_n \frac{dn(x)}{dx}, \tag{3.25}$$

where F is the electric field, μ_n and D_n are the electron mobility and electron diffusion coefficient respectively. If we consider uniform electric field approximation throughout the entire active layer thickness (L) then electrostatic field can be written as:

$$F = \frac{V - V_{bi}}{L}, \tag{3.26}$$

where V is the applied bias voltage and V_{bi} is the built-in potential of the device that can be calculated from the work functions difference of the electrodes.

If we use Eq. (3.25) and (3.26) and replace the values in Eq. (3.24) then it becomes

$$\mu_n F \frac{dn(x)}{dx} + D_n \frac{d^2 n(x)}{dx^2} - \frac{n(x)}{\tau_n} = 0$$

$$\Rightarrow \mu_n F \frac{dn(x)}{dx} + \mu_n V_t \frac{d^2 n(x)}{dx^2} - \frac{n(x)}{\tau_n} = 0;$$ (Diffusion coefficient is assumed to be independent of n and can be determined using Einstein's relation: $\frac{D_n}{\mu_n} = \frac{kT}{e} = V_t$)

$$\Rightarrow \frac{d^2 n(x)}{dx^2} + \frac{F}{V_t}\frac{dn(x)}{dx} - \frac{n(x)}{L_n^{\,2}} = 0; \qquad L_n = \text{Diffusion Length}$$

Thus, the solution of electron density would be:

$$n(x,V) = A_1 \exp(m_1 x) + A_2 \exp(m_2 x), \tag{3.27}$$

where, $m_{1,2} = -\frac{F}{2V_t} \pm \sqrt{\left(\frac{F}{2V_t}\right)^2 + \frac{1}{L_n{}^2}}$

The fermi position at the two contacts is determined by the metal work functions. Thus, the constants A_1 and A_2 can be determined by the following two boundary conditions,

$$n(0) = N_c \exp\left(-\frac{E_g - \phi_2}{eV_t}\right), \tag{3.28}$$

$$n(L) = N_c \exp\left(-\frac{\phi_1}{eV_t}\right), \tag{3.29}$$

where, N_c is the effective density of states in the conduction band.

Applying boundary conditions in Eq. (3.27), the expressions of A_1 and A_2 are,

$$A_1 = \frac{N_c\left[\exp\left(-\frac{E_g - \phi_2}{eV_t} + m_2 L\right) - \exp\left(-\frac{\phi_1}{eV_t}\right)\right]}{\exp(m_2 L) - \exp(m_1 L)}, \tag{3.30}$$

$$A_2 = \frac{N_c\left[\exp\left(-\frac{\phi_1}{eV_t}\right) - \exp\left(-\frac{E_g - \phi_2}{eV_t} + m_1 L\right)\right]}{\exp(m_2 L) - \exp(m_1 L)}, \tag{3.31}$$

Similarly, the expression of holes under dark condition is,

$$p(x,V) = B_1 \exp(k_1 x) + B_2 \exp(k_2 x), \tag{3.32}$$

where, $k_{1,2} = \frac{F}{2V_t} \pm \sqrt{\left(\frac{F}{2V_t}\right)^2 + \frac{1}{L_p{}^2}}$ and $L_p = \sqrt{D_p \tau_p}$

The boundary conditions for holes are:

$$p(0) = N_v \exp\left(-\frac{\phi_2}{eV_t}\right), \tag{3.33}$$

$$p(L) = N_v \exp\left(-\frac{E_g - \phi_1}{eV_t}\right), \tag{3.34}$$

where, N_v is the effective density of states in the valence band.

Applying the above boundary conditions in Eq. (3.32), the constants B_1 and B_2 are,

$$B_1 = \frac{N_v\left[\exp\left(-\frac{\phi_2}{eV_t} + k_2 L\right) - \exp\left(-\frac{E_g - \phi_1}{eV_t}\right)\right]}{\exp(k_2 L) - \exp(k_1 L)}, \tag{3.35}$$

$$B_2 = \frac{N_v\left[\exp\left(-\frac{E_g - \phi_1}{eV_t}\right) - \exp\left(-\frac{\phi_2}{eV_t} + k_1 L\right)\right]}{\exp(k_2 L) - \exp(k_1 L)}, \tag{3.36}$$

In the dark condition, recombination current dominates over drift and diffusion current. "Shockley-Read-Hall" recombination (or SHR model) is considered for the recombination current. According to the SHR model, the recombination rate is,

$$R = \frac{np - n_i^2}{\tau_p(n + n') + \tau_n(p + p')}, \tag{3.37}$$

where, n' and p' are the trapped electron and hole concentrations, τ_n and τ_p are the excess electron and hole lifetimes. For simplicity, the trap levels are assumed to be near the middle of the bandgap (i.e. $n' = p' \approx n_i$). Hence, Eq. (3.37) becomes

$$R = \frac{np - n_i^2}{\tau_p(n + n_i) + \tau_n(p + n_i)} \tag{3.38}$$

Thus, the recombination current or dark current will be

$$J_{dark} = J_{rec} = e\int_0^L R(x)dx \tag{3.39}$$

Note that one has to substitute the values of n and p from equations (3.27) and (3.32) into equation (3.38) and perform numerical integration of equation (3.39) in order to calculate the dark current, J_{dark}. Fig. 3.3 shows the numerical simulation of the equation (3.39). The simulation curve (black solid line) fits well with the experimental dark current curve (blue solid line) [59]. Therefore, this model is taken as the dark current model for further analysis.

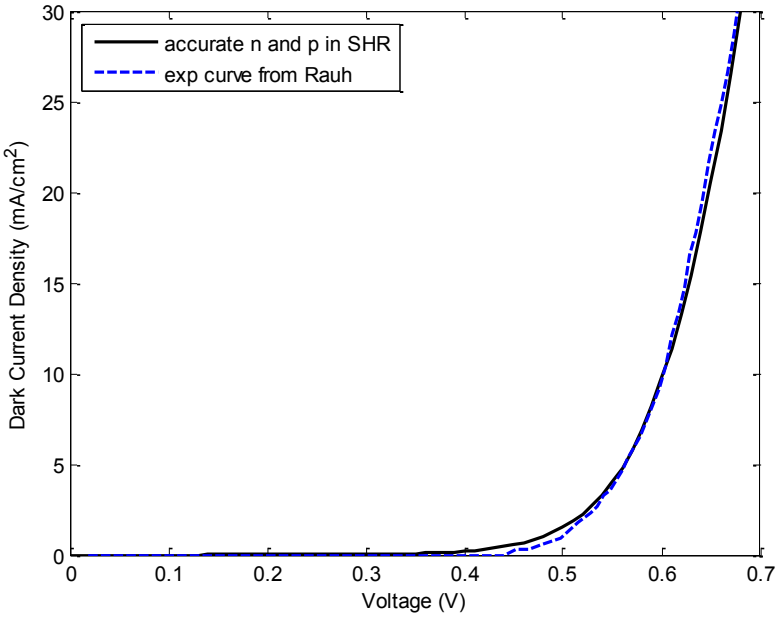

Figure 3.3 Experimental dark current (blue dashed line) [59] and the derived dark current model (black solid line) as a function of applied voltage

The parameters taken to plot the graph are given in the Table 3.1. The electron and hole lifetimes are kept fixed at 1μs and 3 μs respectively.

As shown in figure 3.1, holes are the majority carrier in the first half of the active layer (0 to L/2) and electrons are the majority carriers in the other half (L/2 to L). Thus, the recombination rate for the excess minority carrier electrons can be written as, $R_n = \frac{n - n_0}{\tau_n}$ for *x=0 to L/2* provided $\phi_1 \approx \phi_2$, where τ_n is the electron lifetime. Similarly, recombination

rate for excess minority carrier holes, $R_p = \frac{p - p_0}{\tau_p}$ for $x=L/2$ *to* L, where τ_p is the hole lifetime.

Therefore, the recombination current due to the electron is

$$J_{rn} = e \int_0^{L/2} \frac{n(x,V) - n_0(x)}{\tau_n} dx \,, \tag{3.40}$$

$n(x,V)$ is the voltage and position dependent electron concentration given in Eq. (3.27) and if V is set to zero in this expression then $n_0(x)$ can be found.

$$n_0(x) = n(x,0) = A_1 \exp(m_{01}x) + A_2 \exp(m_{02}x) \,, \tag{3.41}$$

where, $m_{01,02} = -\frac{F_0}{2V_t} \pm \sqrt{\left(\frac{F_0}{2V_t}\right)^2 + \frac{1}{{L_n}^2}}$, $F_0 = \frac{-V_{bi}}{L}$ and A_1, A_2 are given in Eq. (3.30) and (3.31) respectively. Now, if Eq. (3.40) is integrated after replacing these values then the recombination current would be,

$$J_{rn} = \frac{e}{\tau_n} \left[\begin{array}{l} \frac{A_1}{m_1}\left\{\exp\left(m_1 \frac{L}{2}\right) - 1\right\} + \frac{A_2}{m_2}\left\{\exp\left(m_2 \frac{L}{2}\right) - 1\right\} \\ -\frac{A_1}{m_{01}}\left\{\exp\left(m_{01} \frac{L}{2}\right) - 1\right\} - \frac{A_2}{m_{02}}\left\{\exp\left(m_{02} \frac{L}{2}\right) - 1\right\} \end{array} \right] \tag{3.42}$$

Similarly, recombination current due to hole would be,

$$J_{rp} = e \int_{L/2}^{L} \frac{p(x,V) - p_0(x)}{\tau_p} dx \,, \tag{3.43}$$

$p(x,V)$ is the voltage and position dependent hole concentration given in Eq. (3.32) and if V is set to zero in this expression then $p_0(x)$ can be found.

$$p_0(x) = p(x,0) = B_1 \exp(k_{01}x) + B_2 \exp(k_{02}x) \,, \tag{3.44}$$

where, $k_{01,02} = \frac{F_0}{2V_t} \pm \sqrt{\left(\frac{F_0}{2V_t}\right)^2 + \frac{1}{{L_p}^2}}$, $F_0 = \frac{-V_{bi}}{L}$ and B_1, B_2 are given in Eq. (3.35) and Eq. (3.36) respectively. Therefore, from Eq. (3.43),

$$J_{rp} = \frac{e}{\tau_p}\left[\begin{array}{l} \frac{B_1}{k_1}\left\{\exp\left(k_1 L\right) - \exp\left(k_1 \frac{L}{2}\right)\right\} + \frac{B_2}{k_2}\left\{\exp\left(k_2 L\right) - \exp\left(k_2 \frac{L}{2}\right)\right\} \\ -\frac{B_1}{k_{01}}\left\{\exp\left(k_{01} L\right) - \exp\left(k_{01} \frac{L}{2}\right)\right\} - \frac{B_2}{k_{02}}\left\{\exp\left(k_{02} L\right) - \exp\left(k_{02} \frac{L}{2}\right)\right\} \end{array}\right] \tag{3.45}$$

Thus, the total recombination current would be the sum of Eq. (3.42) and (3.45)

$$J_{dark} = J_{rn} + J_{rp} \tag{3.46}$$

Fig. 3.4 represents the comparison between the experimental data obtained by Rauh et al. [59] vs the curve derived from the analytical model simplifying the Shockley-Hall-Read recombination method.

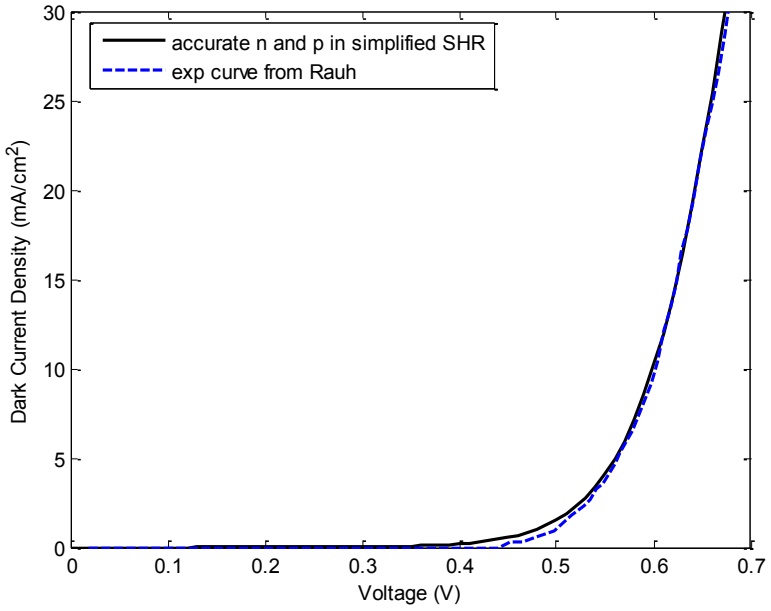

Figure 3.4 Experimental dark current Rauh et al. [59] (blue dashed line) and the derived dark current from simplified SHR (black solid line) as a function of voltage

The parameters taken are shown in the Table 3.1. The value for electron and hole lifetimes are kept constant at 3 μs.

3.2.3 Approximated carrier concentration assuming uniform quasi-fermi levels

Fig. 3.5 shows the energy band diagram for an applied voltage, V. Once we apply an external voltage in the system, this voltage creates a separation of fermi levels called quasi-fermi levels and reduces the tilt of the bands (i.e. the electric field of the layer). It is obvious from the figure that quasi-fermi levels for both electrons (E_{Fn}) and holes (E_{Fp}) coincide with each other in the contacts, yet in most part of the blend thickness the difference remains the same.

$$E_{Fn} - E_{Fp} = eV \tag{3.47}$$

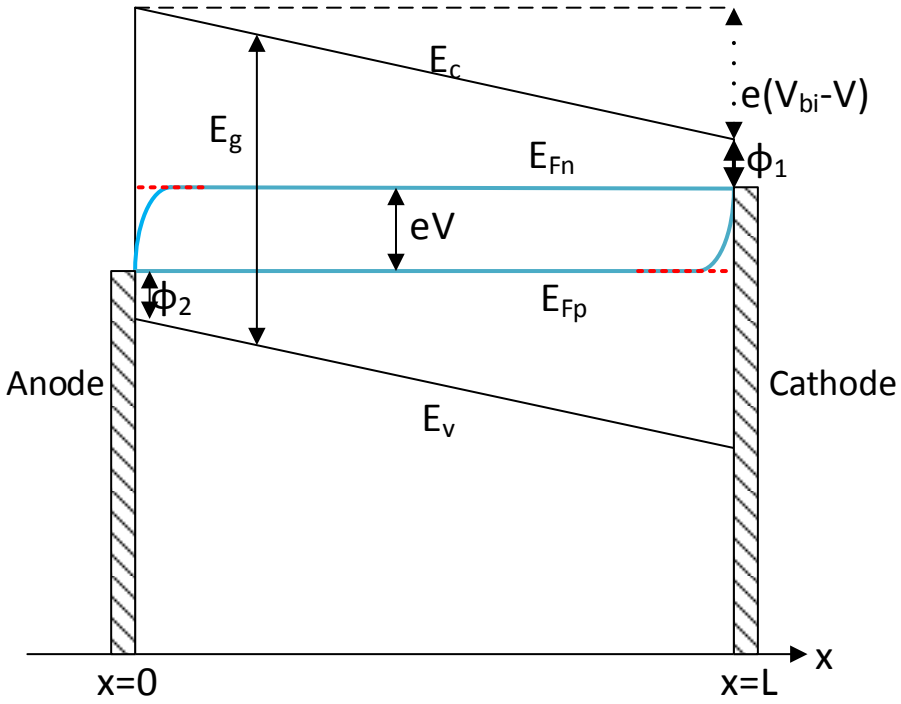

Figure 3.5 Energy band diagram for applied bias (V)

Therefore, in this method a constant difference among quasi-fermi levels all over the blend thickness (shown in red dashed lines) is considered. Thus, the fermi level for electrons can be defined as

$$E_{Fn}(x=0) = eV + \phi_2 \tag{3.48}$$

$$E_{Fn}(x=L)=E_g-\phi_1 \tag{3.49}$$

Hence, fermi level for electrons can be expressed as follows

$$E_{Fn}(x,V)=E_{Fn}(0)+\frac{E_{Fn}(L)-E_{Fn}(0)}{L}x$$

$$=eV+\phi_2+\frac{E_g-\phi_1-eV-\phi_2}{L}x$$

$$E_{Fn}(x,V)=eV+\phi_2+e\frac{V_{bi}-V}{L}x \tag{3.50}$$

Thus, electron concentrations can be obtained from the following equation

$$n(x,V)=n_i\exp\left(\frac{E_{Fn}(x)-E_{Fi}}{V_t}\right)$$

$$=n_i\exp\left(\frac{eV+\phi_2+e\frac{V_{bi}-V}{L}x-\frac{E_g}{2}}{eV_t}\right)$$

$$n(x,V)=n_i\exp\left(-\frac{E_g-2\phi_2}{2eV_t}\right)\exp\left(\frac{V}{V_t}\right)\exp\left(\frac{V_{bi}-V}{LV_t}x\right) \tag{3.51}$$

Similarly, for holes we can get

$$E_{Fp}(0)=\phi_2 \tag{3.52}$$

$$E_{Fp}(L)=E_g-\phi_1-eV \tag{3.53}$$

$$E_{Fp}(x,V)=\phi_2+\frac{e(V_{bi}-V)}{L}x \tag{3.54}$$

$$p(x,V)=n_i\exp\left(\frac{E_g-2\phi_2}{2eV_t}\right)\exp\left(-\frac{V_{bi}-V}{LV_t}x\right) \tag{3.55}$$

The dark current due to the Shockley-Hall-Read recombination can be calculated as

$$J_{dark} = e\int_0^L R dx \tag{3.56}$$

where R is the SHR recombination rate that can be defined as

$$R = \frac{np - n_i^{\,2}}{\tau_{p0}(n + n_i) + \tau_{n0}(p + n_i)}$$

If n and p are replaced from Eq. (3.51) and (3.55) respectively in Eq. (3.56) then integrated throughout the entire active layer with respect to position then dark current will be obtained.

Fig. 3.6 shows the numerical solution of Eq. (3.56) and displays a comparison with the empirical data [59].

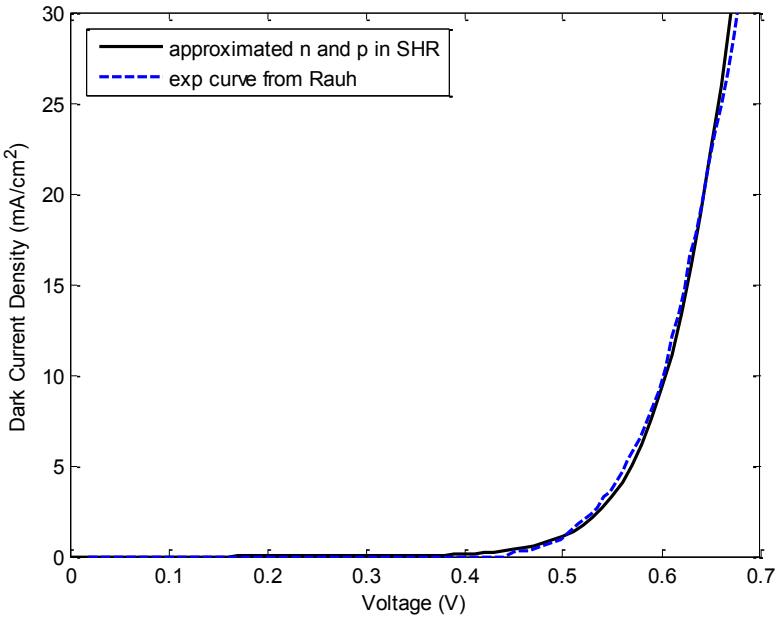

Figure 3.6 Empirical dark current curve Rauh et al. [59] (blue dashed line) and the derived dark current (black solid line) as a function of voltage

The parameters used to plot the above figure are given in Table 3.1. The electron and hole lifetimes are 3 μs and 2 μs respectively.

The recombination current due to electron can be simplified by using simplified SHR equation,

$$J_{rn} = e\int_0^{L/2} \frac{n(x,V)-n_0(x)}{\tau_n}dx \text{, where } n_0(x) = n(x,0) = n_i \exp\left(-\frac{E_g - 2\phi_2}{2eV_t}\right)\exp\left(\frac{V_{bi}}{LV_t}x\right)$$

$$= \frac{e}{\tau_n}\int_0^{L/2} \left[\begin{array}{l} n_i \exp\left(-\frac{E_g - 2\phi_2}{2eV_t}\right)\exp\left(\frac{V}{V_t}\right)\exp\left(\frac{V_{bi}-V}{LV_t}x\right) \\ -n_i \exp\left(-\frac{E_g - 2\phi_2}{2eV_t}\right)\exp\left(\frac{V_{bi}}{LV_t}x\right) \end{array}\right] dx$$

$$J_{rn} = en_i \exp\left(-\frac{E_g}{2eV_t}\right)\left[\frac{1}{\tau_n}\exp\left(\frac{\phi_2}{eV_t}\right)\right]\left[\begin{array}{l} \frac{LV_t}{V_{bi}-V}\exp\left(\frac{V}{V_t}\right)\left\{\exp\left(\frac{V_{bi}-V}{2V_t}\right)-1\right\} \\ -\frac{LV_t}{V_{bi}}\left\{\exp\left(\frac{V_{bi}}{2V_t}\right)-1\right\} \end{array}\right] \quad (3.57)$$

Again, recombination current for holes would be

$$J_{rp} = e\int_{L/2}^{L} \frac{p(x)-p_0(x)}{\tau_p}dx \qquad \text{where } p_0(x) = p(x,0) = n_i \exp\left(\frac{E_g - 2\phi_2}{2eV_t}\right)\exp\left(-\frac{V_{bi}}{LV_t}x\right)$$

$$= \frac{en_i}{\tau_p}\exp\left(\frac{E_g - 2\phi_2}{2eV_t}\right)\left[\begin{array}{l} -\frac{LV_t}{V_{bi}-V}\left\{\exp\left(-\frac{V_{bi}-V}{V_t}\right)-\exp\left(-\frac{V_{bi}-V}{2V_t}\right)\right\} \\ +\frac{LV_t}{V_{bi}}\left\{\exp\left(-\frac{V_{bi}}{V_t}\right)-\exp\left(-\frac{V_{bi}}{2V_t}\right)\right\} \end{array}\right]$$

$$= en_i \exp\left(-\frac{E_g}{2eV_t}\right)\left[\frac{1}{\tau_p}\exp\left(\frac{\phi_1}{eV_t}\right)\right]\left[\begin{array}{l} \frac{LV_t}{V_{bi}-V}\exp\left(\frac{V}{V_t}\right)\left\{\exp\left(\frac{V_{bi}-V}{2V_t}\right)-1\right\} \\ -\frac{LV_t}{V_{bi}}\left\{\exp\left(\frac{V_{bi}}{2V_t}\right)-1\right\} \end{array}\right] \quad (3.58)$$

So, the total dark current will be the sum of equation (3.57) and (3.58)

$$J_{dark} = en_i \exp\left(-\frac{E_g}{2eV_t}\right)\left[\frac{1}{\tau_n}\exp\left(\frac{\phi_2}{eV_t}\right)+\frac{1}{\tau_p}\exp\left(\frac{\phi_1}{eV_t}\right)\right]\left[\begin{array}{l}\dfrac{LV_t}{V_{bi}-V}\exp\left(\dfrac{V}{V_t}\right)\left\{\exp\left(\dfrac{V_{bi}-V}{2V_t}\right)-1\right\} \\ -\dfrac{LV_t}{V_{bi}}\left\{\exp\left(\dfrac{V_{bi}}{2V_t}\right)-1\right\}\end{array}\right] \tag{3.59}$$

Figure 3.7 shows the experimental dark current curve (blue dashed line) and the derived dark current curve (solid black line) in equation (3.59)

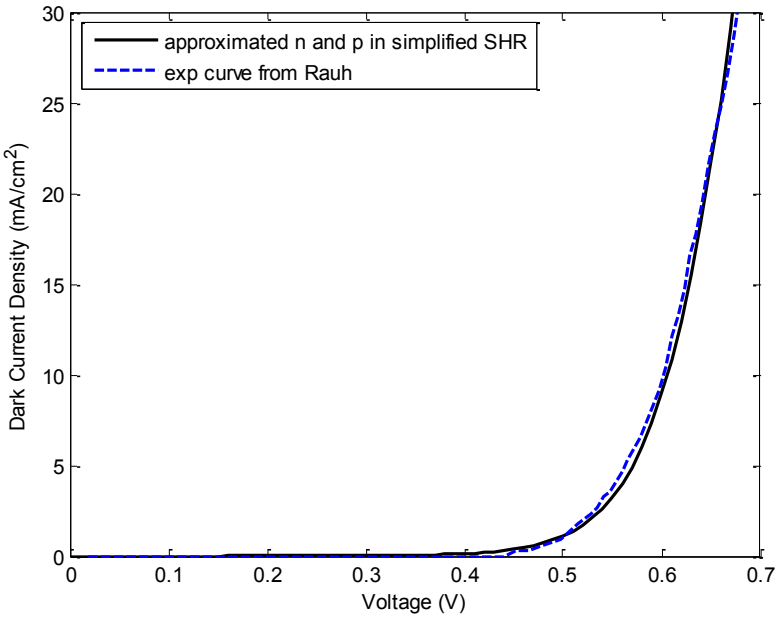

Figure 3.7 Experimental graph (blue dashed line) from Rauh et al. [59] and the derived dark current (black solid line) vs applied voltage

The parameters used to plot the figures are written in Table 3.1. The electron and hole lifetimes are kept fixed at 4 μs and 3 μs.

3.3 Results and discussions

In this chapter, different dark current models are examined and observed as a function of the external voltage in BHJ organic solar cells by comparing the model calculations with recently published experimental results. The various parameters of the P3HT:$PC_{61}BM$ BHJ organic solar cells are given in Table 1. The effective bandgap is the difference between acceptor LUMO level and donor HOMO level. Unless otherwise stated, the parameters shown in Table 1 are the fixed parameters used in all model calculations.

Table 3.1 Parameters used to calculate the J-V characteristics of the organic solar cell

Parameters	Values
Effective bandgap, E_g	1.0 eV
Effective density of states in conduction (valence) band, N_c (N_v)	2×10^{20} cm^{-3}
Mobility of electron, μ_n	2×10^{-3} cm^2/V-s
Mobility of hole, μ_p	2×10^{-4} cm^2/V-s
Electron (Hole) injection barrier, ϕ_1 (ϕ_2)	0.1 eV
Series area resistance, R_s	1 Ω-cm^2
Parallel area resistance, R_p	10^6 Ω-cm^2

3.3.1 Dark current density

Fig. 3.8 (a) and 3.8 (b) show the dark current versus external voltage of a P3HT:$PC_{61}BM$ solar cell. The experimental data are extracted from Refs. [59] and [60]. The active layer thickness, L is 200 nm [59]. The symbols, dashed, dotted, solid, and dash-dotted lines represent experimental results, drift-diffusion model of Kumar el al. [14], present model fit to experimental data of Eqns. (3.38), (3.45) and (3.58) respectively. The common diode equation are also shown in figures (blue solid square symbolic line). The ideality factor, n = 1.67 and 1.9 and reverse saturation current density, $J_o = 15\times10^{-6}$ mA/cm^2 and 20×10^{-6} mA/cm^2 are taken in Figs. 3.8(a) and 3.8(b) respectively. As evident from Figure 3.8, the dark current models considering the SRH recombination provide better fittings. The results of the equations (3.38) and (3.45) are almost identical because of symmetrical carrier

profile across the active layer ($\phi_1 = \phi_2$). The best fitted parameters in Figure 3.8 are; $\mu_p = 2\times10^{-4}$ cm^2/Vs, $\mu_n = 2\times10^{-3}$ cm^2/Vs, $R_s = 1$ Ω-cm^2. The carrier lifetimes, $\tau_n = \tau_p = 3$ and 6 μs in Figs. 3.8(a) and 3.8(b) respectively. The drift-diffusion model of Kumar el al. [14] shows much higher dark current than the experimental observation.

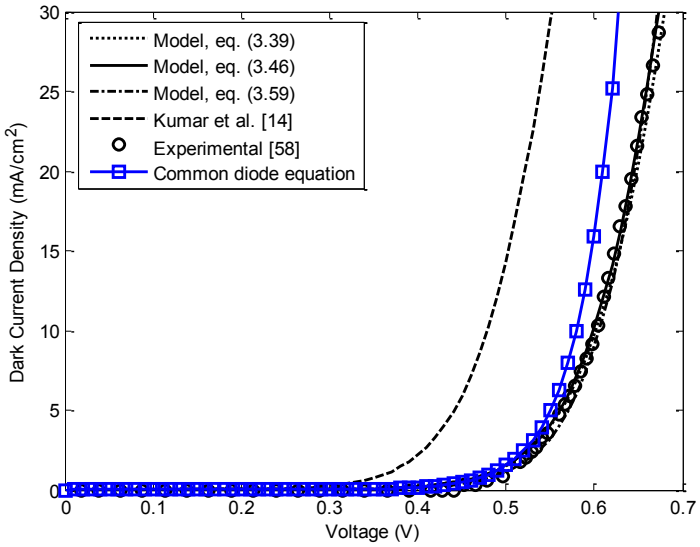

(a)

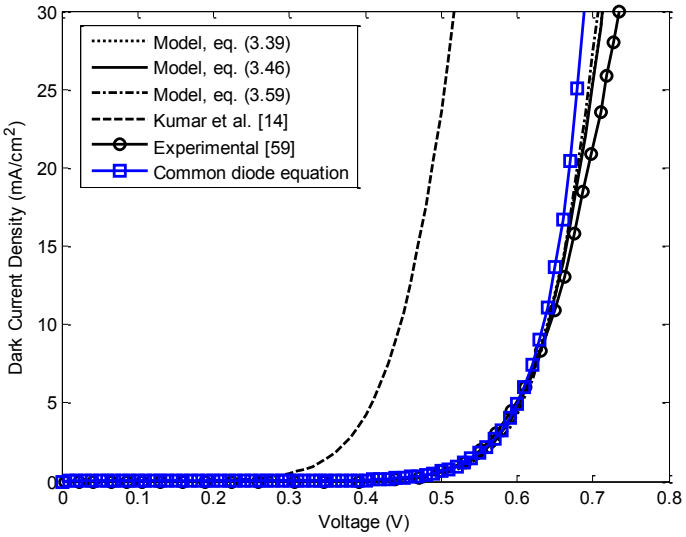

(b)

Figure 3.8 Dark current-voltage characteristics of P3HT:PCBM solar cells

The dark current as a function of the external voltage of a PTB7:$PC_{71}BM$ (poly[[4,8-bis[(2-ethylhexyl)oxy]benzo[1,2-b:4,5-b′]dithiophene-2,6-diyl][3-fluoro-2-[(2-ethylhexyl)carbonyl] thieno [3,4-b] thiophenediyl]]) solar cell is shown in Figure 3.9. The experimental data are extracted from Refs. [59]. As like P3HT:$PC_{61}BM$ solar cell, the SRH recombination is the main source of dark current in PTB7:$PC_{71}BM$ solar cells. The best fitted values of carrier lifetimes $\tau_n = \tau_p = 45$ μs. The ideality factor, $n = 2.1$ and reverse saturation current density, $J_o = 15\times10^{-6}$ mA/cm^2 are considered for the common diode curve All other parameters in Figure 3.9 are the same as in Figure 3.8. Since the results of the equations (3.39) and (3.46) are almost identical and show the best fit to the experimental data, equation (3.46) is used for calculating the dark current in the rest of this thesis.

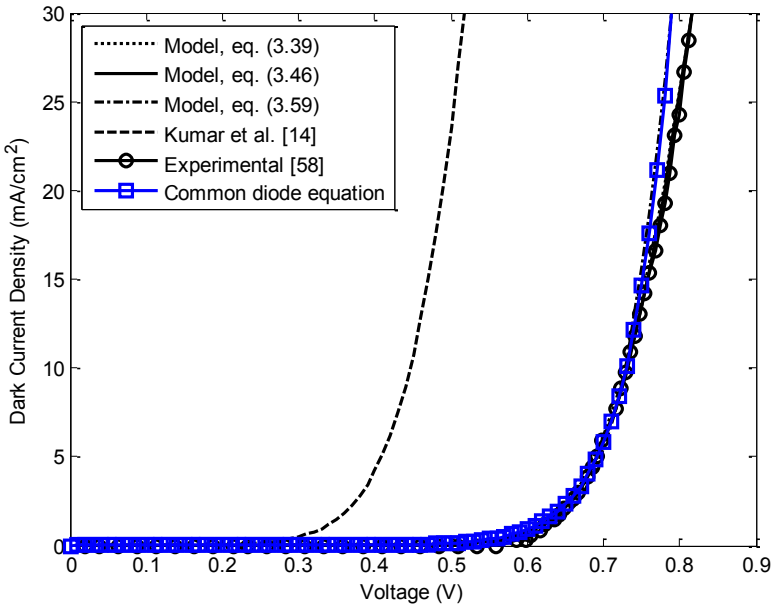

Figure 3.9 Dark current-voltage characteristics of a PTB7:$PC_{71}BM$ solar cell.

3.3.2 Energy band diagram

Fig. 3.10 represents the energy band diagram in the active blend layer of the BHJ solar cell. The parameters used to draw the energy band diagram such as energy bandgap, effective density of states in conduction (valence) band, mobility of electrons (holes), electron (hole)

injection barrier are taken from Table 3.1. The electron and hole lifetimes are kept constant at 1 μs.

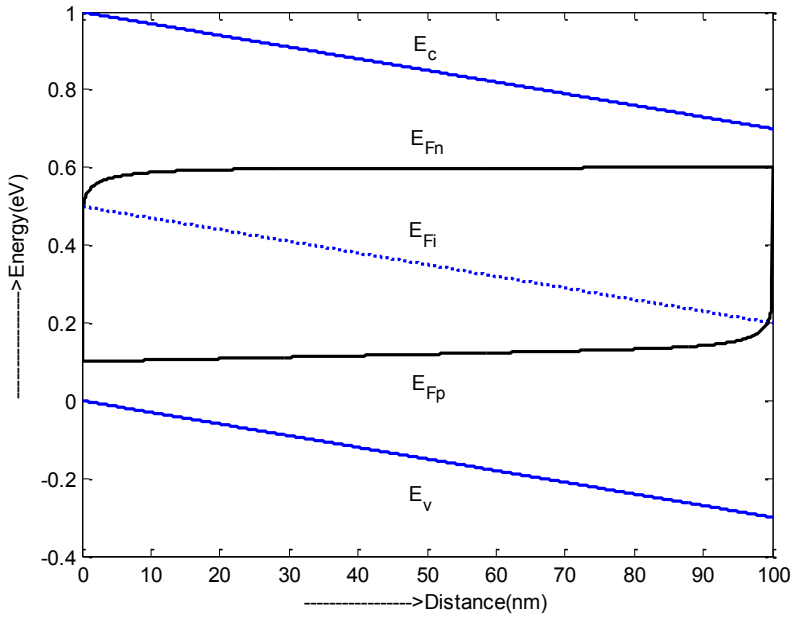

Figure 3.10 Energy band diagram showing the quasi-Fermi levels for both electron and holes for an external bias of 0.5 V at thermal equilibrium

The figure shows that the quasi fermi levels (E_{Fn} and E_{Fp}) are almost uniform throughout the entire blend region except near the two sides of the layer. Therefore, for simplicity, an uniform quasi-fermi levels can be assumed to approximate the carrier concentration. Both electron and hole fermi levels are joined together at the two ends. From the figure it can be observed that in the first half of the active layer the difference from the intrinsic fermi level to the hole fermi level is much greater than that of the electron fermi level.

3.3.3 Recombination rate

Fig. 3.11 shows the relative recombination rate for different biases in the active layer of the solar cell at the dark condition. A very sharp peak occurs in the middle of the blend

layer length which means recombination takes place mostly in the middle. As the voltage increases, the curve shifts left due to the difference in the carrier mobility. The parameters: E_g, N_c, N_v, μ_n, μ_p, ϕ_1, ϕ_2 are taken from Table 3.1. The active layer thickness, L is considered to be 100 nm. Electron and hole lifetimes are fixed at 1 μs.

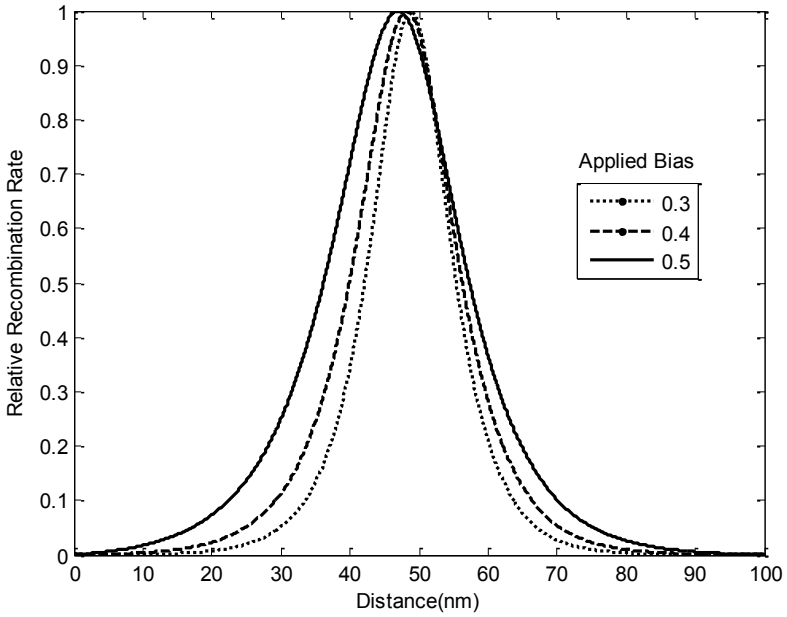

Figure 3.11 Relative recombination rate with respect to distance for different applied voltages (dotted line, dashed line and solid line are for 0.3, 0.4, 0.5 voltages respectively)

3.3.4 Carrier concentration

Fig. 3.12(a) and 3.12(b) represent electron and hole concentrations while the solar cell is in the dark condition for different applied biases. At zero bias, the carriers increase linearly in logarithmic scale because the carrier profile is exponential (Eq. 3.2). As the voltage increases, the built-in-electric field is reduced and the carrier profiles follow the quasi fermi levels (Fig 3.10). Nevertheless, the two edges of the active layer have the same electron and hole concentrations since $\phi_1 = \phi_2$. All the parameters are taken from Table 3.1. The electron and hole lifetimes are kept constant at 1 μs.

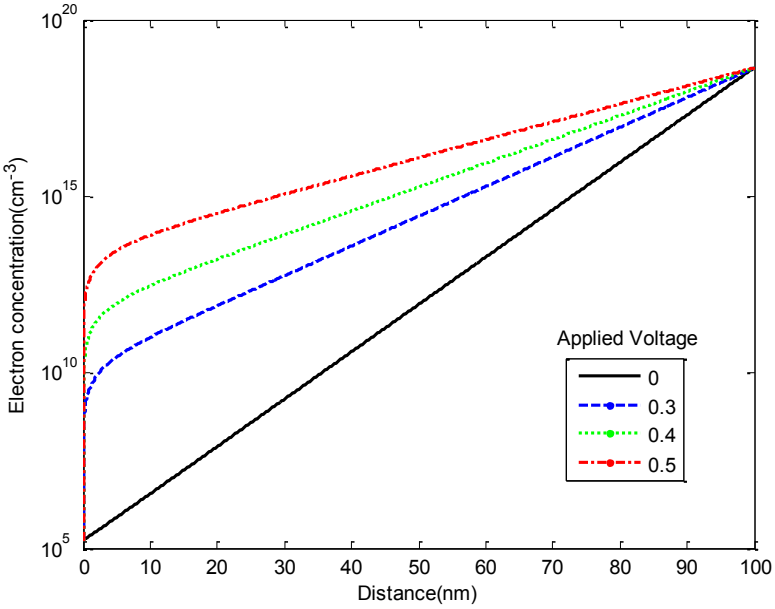

(a)

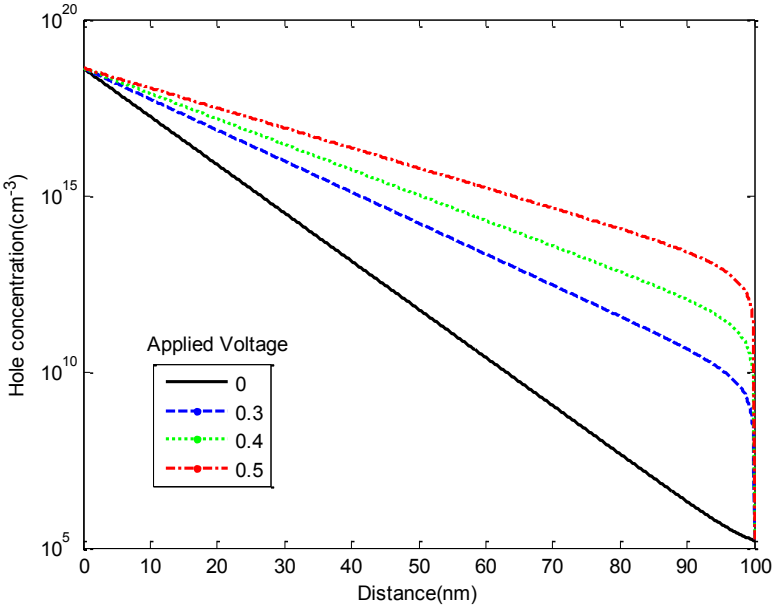

(b)

Figure 3.12 (a) Electron concentration (b) Hole concentration for various applied voltages under dark condition.

3.4 Summary

In this chapter, three models have been proposed assuming different boundary conditions for calculating dark current. At the same time a comparative analysis has been performed at the end to check the accuracy of each model. Among the three models, the dark current models considering the SRH recombination with accurate n and p provide better fittings with the experimental results. The accurate expression of R and its simplified version give almost identical results because of the symmetrical carrier profiles across the active layer ($\phi_1 = \phi_2$).

CHAPTER 4: PHOTOCURRENT MODEL OF BHJ

4.1 Introduction

In this chapter, an analytical model for voltage-dependent photocurrent is presented considering electric field dependent escape probability. When a solar cell is illuminated in the sunlight, it absorbs light particles or photons if the photon energy is greater than or equal to the LUMO and HOMO difference of the active layer. As it is mentioned earlier, the potential difference between donor (conjugated polymer) and acceptor (soluble fullerene derivative) near the heterojunction helps the excitons to dissociate. Photocarriers are generated if the diffusion length of the bound EHPs is greater than the interface length that an exciton needs to travel. In BHJ polymer solar cells, donor and acceptor materials are mixed together to spread dissociation sites in the entire blend layer (P3HT:PCBM). The probability of EHPs separation is known as escape probability. The dissociation of the bound EHPs is determined by the Modified Braun Model, which supports the exact extension of Onsager theory at low electric field. An exponential photon absorption and actual solar spectrum are also taken into account to compute the photocurrent densities at various output voltages. The incident photon flux, AM 1.5 global spectrum, is taken from the ASTM G-173-03 standard [62]. The total load current is calculated including the effects of voltage dependent forward dark current which has been developed in the previous chapter. The developed model is then compared with the published experimental data. This chapter combines selected material from my published journal paper.[2]

4.2 Modified Braun model

Braun [63] proposed an empirical model to compute electric field-dependent escape probability, assuming geminate recombination at a nonzero reaction radius. The minimum distance required for bound electron and hole is called the reaction radius. Onsager assumed zero reaction radius for geminate recombination [18]. This assumption leads to a

[2] Saleheen, M., Arnab, S. M., & Kabir, M. Z. (2016). Analytical Model for Voltage-Dependent Photo and Dark Currents in Bulk Heterojunction Organic Solar Cells. *Energies*, *9*(6), 412.

.

very low separation rate as compared to the observed escape probability in P3HT:PCBM blends. However, it has been shown that bound electron and hole recombine at a nonzero distance [48]. Thus, Onsager model cannot explain the exact behavior of the geminate pairs under the influence of a built-in potential.

Based on the theory that geminate recombination occurs at a nonzero reaction radius, Braun proposed an empirical model to measure the electric field dependent escape probability. The expression for electric field-dependent dissociation rate proposed by Braun is given by [48]

$$M(F) = \frac{K_d(F)}{K_d(F) + K_f} \tag{4.1}$$

where, $M(F)$ is the field dependent escape probability, K_d is the separation rate, $K_f\left(=\frac{S}{r_0}\right)$ is the recombination rate of bound EHPs, r_0 is the initial separation of electron and hole (or reaction radius) and S denotes the reactivity parameter. The relative velocity between bound electron and hole at the reaction radius is known as the reactivity parameter. Later, Wojcik et al. [18] showed that Eq. (4.1) is not valid because both recombination and separation processes are assumed to follow exponential kinetics. They showed that Modified Braun model agrees well with the exact extension of Onsager theory except at very high electric field. The Modified Braun's model expressed K_d as below [18]

$$K_d(F) = \frac{Dr_c}{{r_0}^3 e^{r_c/r_0}} J_1\left[2\sqrt{-2b}\right] \Big/ \sqrt{-2b} \tag{4.2}$$

where, D is the sum of the diffusion coefficients of electrons and holes in respective mediums, $r_c\left(=e^2/4\pi\varepsilon_0\varepsilon_r kT\right)$ is the Onsager radius, J_1 is the first order Bessel function, $\varepsilon_0\varepsilon_r$ is the effective dielectric constant of the blend, e is the elementary charge, k is the Boltzmann constant, T is the absolute temperature and the reduced field, $b = e^3F/8\pi\varepsilon_0\varepsilon_r k^2T^2$.

Therefore, the Eq. (4.1) will become

$$M(F)=\left[1+\frac{K_f r_0^{\,3} e^{r_c/r_0}}{D r_c J_1\left[2\sqrt{-2b}\right]/\sqrt{-2b}}\right] \tag{4.3}$$

4.3 Electric field dependent photocurrent model

To achieve a physics based photocurrent model, the continuity equation needs to be solved to find out the photo-generated carrier concentration and hence the total photo-current density. Few assumptions have been made to derive this model: (i) uniform electric field F in the blend layer, (ii) constant drift mobility (μ) and a single lifetime (τ) for both holes and electrons in the donor and acceptor, respectively.

4.3.1 Net current density

The total net current density from a solar cell is [64] given by

$$J(V)=J_{dark}(V)+\frac{V-JR_s}{R_p}-J_{ph}(V) \tag{4.4}$$

where, J_{dark} is the dark current density, J_{ph} is the photocurrent density, R_s and R_p is the series and shunt area resistances respectively.

4.3.2 Photocarrier generation rate

The electron-hole pair generation rate (G) in the P3HT:PCBM blend layer can be expressed as [65] below

$$G(\lambda,V)=\alpha(\lambda)[1-R(\lambda)]\lambda I_0(\lambda)M/hc \tag{4.5}$$

where, I_0 is the intensity of the solar spectra (W/cm^2-nm), c is the speed of light, h is the Plank constant, M is the field dependent dissociation efficiency, R is the reflectance or the loss factors, $\alpha(\lambda)$ is the absorption coefficient of the blend and λ is the incident photon wavelength.

4.3.3 Field dependent photocurrent density

When the solar cell is illuminated in the sunlight then light particles (i.e. photons) are absorbed in the active layer region and as a result excess carriers are generated. Then these carriers are drifted towards the two electrodes (electrons in the cathode and holes in the anode) due to the strong electric field in the active layer. These excess carrier densities can be calculated from the continuity equation as follows

For electrons,

$$\frac{\partial}{\partial t}(\delta n) = \mu_n F \frac{\partial}{\partial x}(\delta n) + D_n \frac{\partial^2}{\partial x^2}(\delta n) + G\exp[-\alpha(\lambda)x] - R_n, \tag{4.6}$$

Recombination rate, $R_n = \frac{\delta n}{\tau_n}$.

G is the EHP generation rate at $x=0$, $\alpha(\lambda)$ is the absorption coefficient of the blend for the photons of wavelength λ

Under these assumptions the Eq. (4.6) becomes

$$\mu_n F \frac{\partial}{\partial x}(\delta n) + D_n \frac{\partial^2}{\partial x^2}(\delta n) + G_0 \exp[-\alpha(\lambda)x] - \frac{\delta n}{\tau_n} = 0, \tag{4.7}$$

The solution of Eq. (4.7) is

$$\delta n(x,\lambda) = C_1 \exp(m_1 x) + C_2 \exp(m_2 x) + A\exp[-\alpha(\lambda)x], \tag{4.8}$$

where, $m_{1,2} = -\frac{F}{2V_t} \pm \sqrt{\left(\frac{F}{2V_t}\right)^2 + \frac{1}{L_n{}^2}}$

Since the carrier concentrations at the two boundaries are fixed, the boundary conditions for the photogenerated excess carriers are

$$\delta n(0) = 0, \tag{4.9}$$

$$\delta n(L) = 0, \tag{4.10}$$

Applying boundary conditions in Eq. (4.8), the expressions of C_1 and C_2 are,

$$C_1 = \frac{A\left[\exp\left(-\alpha L\right) - \exp\left(m_2 L\right)\right]}{\exp\left(m_2 L\right) - \exp\left(m_1 L\right)}, \tag{4.11}$$

$$C_2 = \frac{A\left[\exp\left(-\alpha L\right) - \exp\left(m_1 L\right)\right]}{\exp\left(m_1 L\right) - \exp\left(m_2 L\right)}, \tag{4.12}$$

$$A = \frac{G\tau_n}{1 - \alpha\mu_n F\tau_n - \left(L_n\alpha\right)^2}, \tag{4.13}$$

Therefore the photocurrent density due to electrons that are travelling towards the back electrode is [19,66],

$$J_n\left(\lambda, V\right) = \frac{e}{L}\mu_n F\int_0^L \delta n dx$$

$$= \frac{e}{L}\mu_n F\left\{\frac{C_1}{m_1}\left[\exp\left(m_1 L\right) - 1\right] + \frac{C_2}{m_2}\left[\exp\left(m_2 L\right) - 1\right] - \frac{A}{\alpha}\left[\exp\left(-\alpha L\right) - 1\right]\right\} \tag{4.14}$$

Similarly, the hole concentration is,

$$\delta p\left(x, \lambda\right) = D_1\exp\left(k_1 x\right) + D_2\exp\left(k_2 x\right) + B\exp\left[-\alpha\left(\lambda\right)x\right], \tag{4.15}$$

where, $k_{1,2} = \frac{F}{2V_t} \pm \sqrt{\left(\frac{F}{2V_t}\right)^2 + \frac{1}{L_p{}^2}}$

$$D_1 = \frac{B\left[\exp\left(-\alpha L\right) - \exp\left(k_2 L\right)\right]}{\exp\left(k_2 L\right) - \exp\left(k_1 L\right)}, \tag{4.16}$$

$$D_2 = \frac{B\left[\exp\left(-\alpha L\right) - \exp\left(k_1 L\right)\right]}{\exp\left(k_1 L\right) - \exp\left(k_2 L\right)}, \tag{4.17}$$

$$B = \frac{G\tau_p}{1 - \alpha\mu_p F\tau_p - \left(L_p\alpha\right)^2}, \tag{4.18}$$

Thus, the photocurrent density due to hole transport,

$$J_p(\lambda,V)=\frac{e}{L}\mu_p F\int_0^L \delta p\,dx$$

$$=\frac{e}{L}\mu_p F\left\{\frac{D_1}{k_1}\left[\exp(k_1 L)-1\right]+\frac{D_2}{k_2}\left[\exp(k_2 L)-1\right]-\frac{B}{\alpha}\left[\exp(-\alpha L)-1\right]\right\} \qquad (4.19)$$

Therefore the total photocurrent density due to the incident photon radiation can be obtained by integrating over all incident photon wavelengths of the solar spectrum, i.e.,

$$J_{ph}(V)=\int_0^\infty \left\{J_n(\lambda,V)+J_p(\lambda,V)\right\}d\lambda \qquad (4.20)$$

Now, if $J_{ph}\,(V)$ is plugged into Eq. (4.4) then total net external current density can be obtained.

4.4 Results and discussions

To validate the model, the dark current expression (derived in Chapter 3) and the photocurrent expression are plugged into the net current density equation (Eq. 4.4) of the solar cell to plot the J-V characteristics of the solar cell and then fitted with the experimental results using the software MATLAB. Besides, the effect of blend thickness, injection barrier and carrier mobility effect on the current density, potential distribution, carrier density distributions and recombination distribution in the layer are also analyzed in this chapter. The parameters used for photocurrent model calculation of the P3HT:$PC_{61}BM$ are given in Table 4.1. Unless otherwise specified, these values are the fixed parameters in all other calculations.

Table 4.1 Parameters used for calculating photo-characteristics of P3HT:$PC_{61}BM$ BHJ organic solar cells.

Parameters	Value
Effective Bandgap, E_g	1 eV
Electron (Hole) injection barrier, ϕ_1 (ϕ_2)	0.1 eV
Effective density of states in conduction (valence) band, N_c (N_v)	2×10^{20} cm^{-3}
Relative dielectric constant ε_r	3.5
Parallel area resistance, R_p	10^6 ohm-cm^2
Initial separation, r_0	1.5 nm

4.4.1 Excess photo carrier concentration

Fig. 4.1(a) and 4.1(b) show the density of electrons and holes for different bias voltages when the solar cell is illuminated. When the solar cell is exposed to sunlight, light particles or photons are absorbed. The photons are absorbed exponentially and thus photocarriers are also generated exponentially. Photogenerated electrons move towards the back electrode and holes move towards the front electrode (radiation receiving electrode). The parameters taken to plot these graphs are shown in Table 4.1.

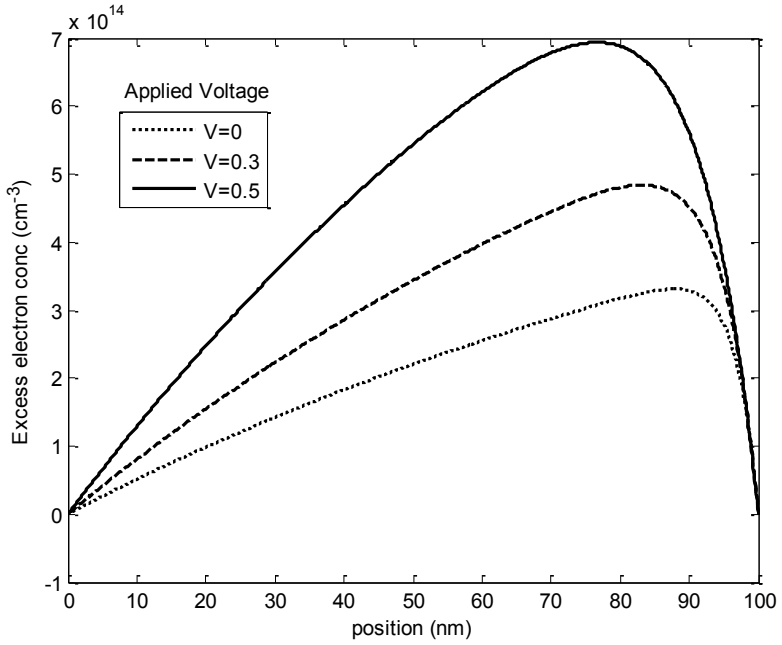

(a)

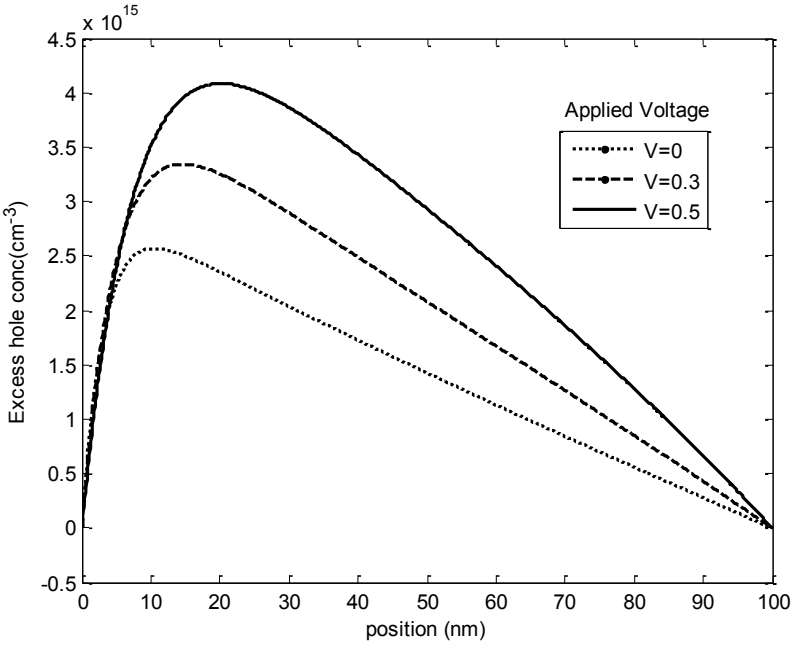

(b)

Figure 4.1 (a) Photo-generated excess electron (b) excess hole concentration for various voltages

4.4.2 J-V characteristics

Figure 4.2 shows the J-V characteristics of P3HT: PCBM solar cells at different sun intensities (i.e. 0.5, 0.75, 1 and 1.4 sun) for L=230 nm. The symbols and black solid lines represent experimental data [53] and model fit, respectively. The analytical model is compared with and justified by fitting the published experimental results. The absorption coefficients of the blends (PCDTBT:$PC_{70}BM$ and P3HT:$PC_{61}BM$) at different wavelengths are taken into account [67,28]. The carrier lifetime and mobility are kept within a suitable range while fitting the experimental results [21,68]. The experimental data for different sun intensities are collected from Shuttle et al. [Fig. 4(a) of Ref. 53]. The exciton dissociation efficiency at the operating voltage is about 87% for $r_0 = 1.5$ nm. In order to ensure the best fit to the experimental results, the electron and hole lifetimes are kept fixed at 2 μs and 18 μs, respectively. The values of other fitting parameters in Fig. 2 are: $\mu_p = 5\times10^{-4}$ cm^2/Vs, $\mu_n = 5\times10^{-3}$ cm^2/Vs, $R_s = 0.3$ Ω-cm^2, and $R = 0.11$. The power conversion efficiency for 1 sun intensity is 2.87%. The analytical model agrees well with the experimental data.

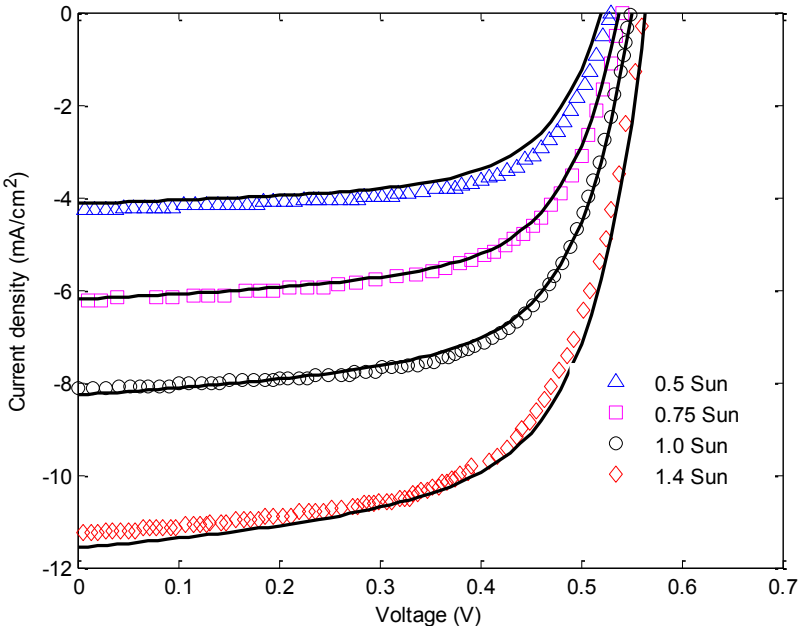

Figure 4.2 Current-voltage characteristics of a P3HT:$PC_{61}BM$ solar cell at different sun intensities. The symbols represent experimental data [53] and solid lines represent the model fit to the experimental data.

4.4.3 Effect of thickness on J-V curves

Figure 4.3 shows the effects of active layer thickness on *J-V* characteristics of PCDTBT:$PC_{71}BM$ solar cells. The symbols and solid lines represent the experimental results [49] and model fit, respectively. The cell performance, particularly the fill factor, deteriorates with increasing the active layer thickness from 70 to 150 nm. Low carrier mobility in PCDTBT are responsible for lower charge collection efficiency in thicker devices. Therefore, the active layer thickness is usually kept around 70-80 nm. The bandgap and dielectric constant (ε_r) of PCDTBT:PCBM blend are 1.2 eV and 3.8. The dissociation efficiencies at maximum power points are 99% and 98.5% for W = 70 nm and W = 150 nm, respectively, which indicates that the dissociation efficiency in PCDTBT:PCBM blend is much higher as compared to P3HT:PCBM blend. This is due to the fact that the dielectric constant for PCDTBT is higher (~3.8) than P3HT (~3.5). Higher dielectric constant reduces the coulombic attraction between the bound EHPs. Initial separation also affects the dissociation rate. The other fitting parameters in Figure 6 are; μ_n = 5 × 10^{-5} cm^2/Vs, μ_p = 6 ×10^{-5} cm^2/Vs, τ_n =13 μs, τ_p = 25 μs, r_0 =1.8 nm, and R_s = 0.3 and 1 Ω-cm^2 for W = 70 and 150 nm, respectively. The fill factor decreases from 67.8 % to 55% by increasing the active layer thickness from 70 nm to 150 nm.

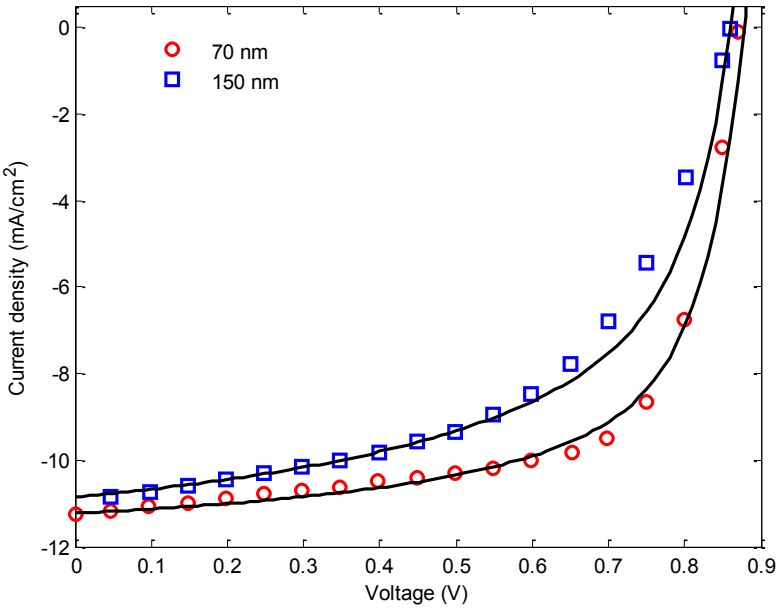

Figure 4.3 Current-voltage characteristics of PCDTBT solar cells for different active layer thicknesses. The symbols and solid lines represent experimental data [49] and model fit to the experimental data, respectively.

4.4.4 Short circuit current density

The effect of blend thickness (L) on short circuit current density (J_{sc}) for a P3HT: PCBM based BHJ solar cell is shown in Figure 4.4. The symbols and solid lines represent the experimental data and the model fit to the experimental results, respectively. The experimental data are extracted from figure 6 of [69]. The short circuit current should increase with increasing the blend thickness because it absorbs more photons (i.e. higher quantum efficiency). On the other hand, the charge collection efficiency decreases with increasing the thickness, which results in lower short circuit current. Thus there exists an optimum thickness that maximizes the short circuit current as shown in Figure 4.4. The fitting parameters in Figure 4.4 are; $\mu_n = 10^{-3}$ cm^2/Vs, $\mu_p = 2 \times 10^{-4}$ cm^2/Vs, $\tau_n = 0.1$ μs, $\tau_p = 0.2$ μs, R = 0.02, and $R_s = 0.5$ Ω-cm^2.

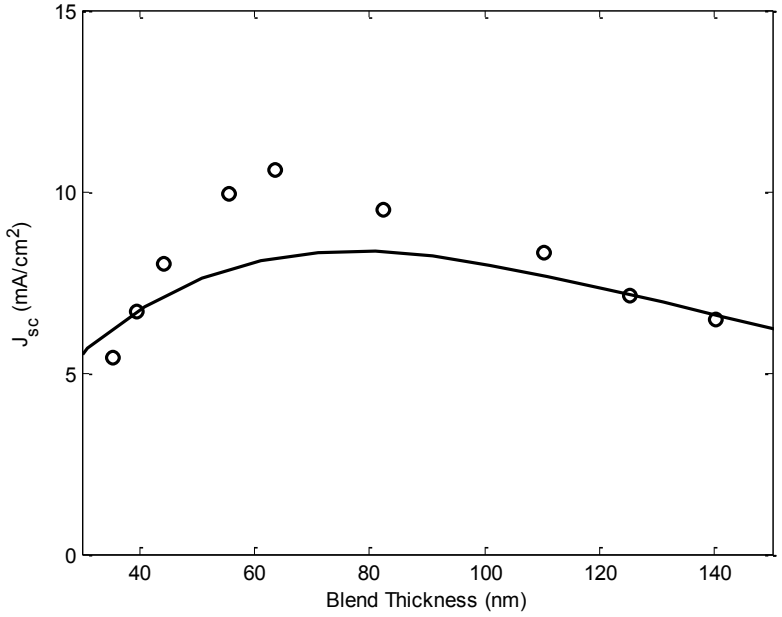

Figure 4.4 Short circuit current density (J_{sc}) versus active layer thickness (L). Symbols: experimental data and solid line: model fit to the experimental results.

4.4.5 Injection barrier effect on J-V curve

The injection barrier heights have a profound effect on the current-voltage characteristics of organic solar cells. The effects of the injection barriers on the current-voltage characteristics of P3HT: PCBM based BHJ solar cells are shown in Figure 4.5. An increase of the electron (hole) injection barrier is equivalent to an increase (decrease) of the cathode (anode) work functions. The built-in potential and electric field decrease with increasing the injection barriers, which reduces the charge collection. Therefore, the short circuit current decreases almost linearly with increasing the barrier height. The open circuit voltage slightly decreases with increasing the barrier heights for low barrier heights (ϕ_1, ϕ_2 < 0.3 eV) and it is equal to the built-in potential for the higher barriers (ϕ_1, $\phi_2 \geq 0.4$ eV). The parameters used in Figure 4.5 are: $\mu_n = 2\times10^{-3}$ cm^2/Vs, $\mu_p = 2\times10^{-4}$ cm^2/Vs, $\tau_n = \tau_p = 20$ μs, L = 180 nm, R = 0, and R_s = 0.3 Ω-cm^2.

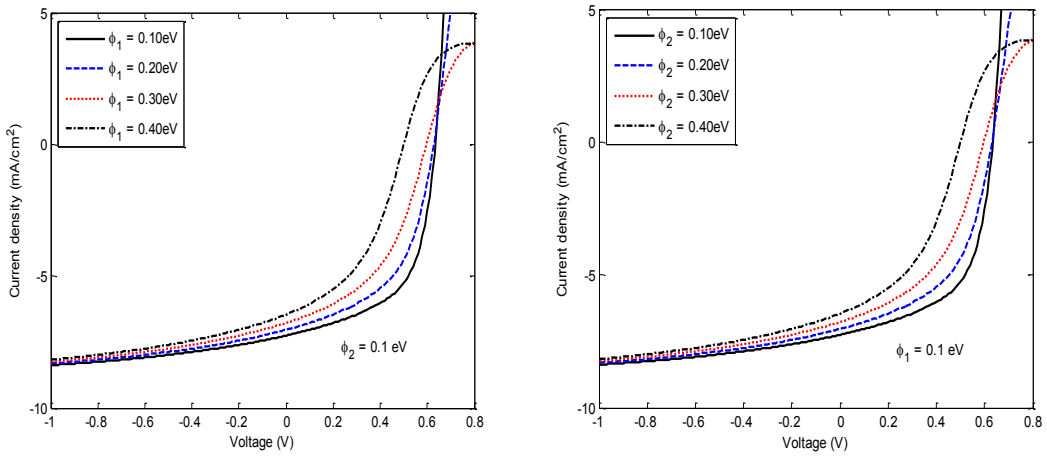

(a) (b)

Figure 4.5 Theoretical net current density versus voltage curves of P3HT:PCBM solar cells for varying (a) electron injection barrier (ϕ_1), and (b) hole injection barrier (ϕ_2).

The difference in quasi-Fermi levels of electrons and holes can be written as [70]

$$E_{Fn} - E_{Fp} = E_g - eV_p - eV_n,$$

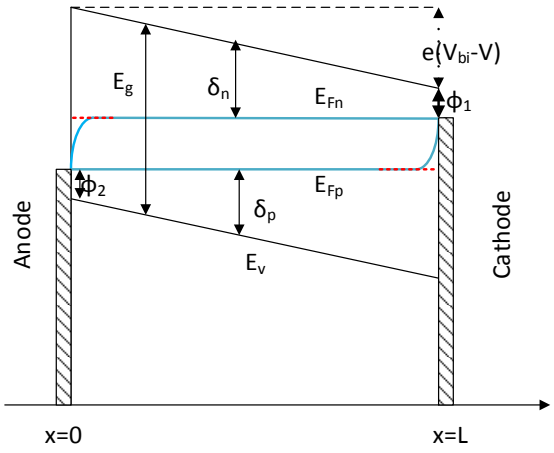

Figure 4.6 Band diagram with symmetrical injection barrier ($\phi_1 = \phi_2$)

where $eV_p\big|_{an} = \phi_2$ and $eV_n\big|_{cat} = \phi_1$. Since $\ln(np) \propto (E_{Fn} - E_{Fp})$, the maximum attainable open-circuit voltage is determined by the largest photo-generated quasi-Fermi level

difference inside the active layer. From the figure it is clear that if the injection barrier is increased then the difference between electron and hole quasi-Fermi levels becomes smaller which in turn decreases the open-circuit voltage. For this reason, with the increase of injection barrier the JV curve shifts from right to left side.

As we can see from the figure that the short circuit current is also decreasing with the increase of injection barrier. This is due to the fact that when the injection barrier is increased electric field becomes weaker and then it affects the charge collection efficiency i.e. the charge will be lost.

4.4.6 Effects of carrier mobility on J-V curve

The theoretical net current versus voltage characteristics of P3HT:PCBM solar cells by varying carrier mobilities are shown in Figure 4.7. All other parameters in Figure 4.7 are the same as in Figure 4.5. The short circuit current decreases drastically with decreasing both electron and hole mobilities though the electron mobility affect more severely than the hole mobility. The open circuit voltage also decreases with decreasing the electron mobility. The hole mobility has almost negligible effect on the open circuit voltage. Both the dark and photocurrent increase with increasing the carrier mobilities. The enhancement of the photocurrent with carrier mobility is higher than that of the dark current, and thus, the net current increases with increasing carrier mobilities. If the mobility is decreased a lot then most of the carriers will recombine before collection i.e. charge collection efficiency is reduced. For this reason, when the carrier mobility is $< 10^{-4}$ $cm^2/V\text{-}s$, the net current decreases.

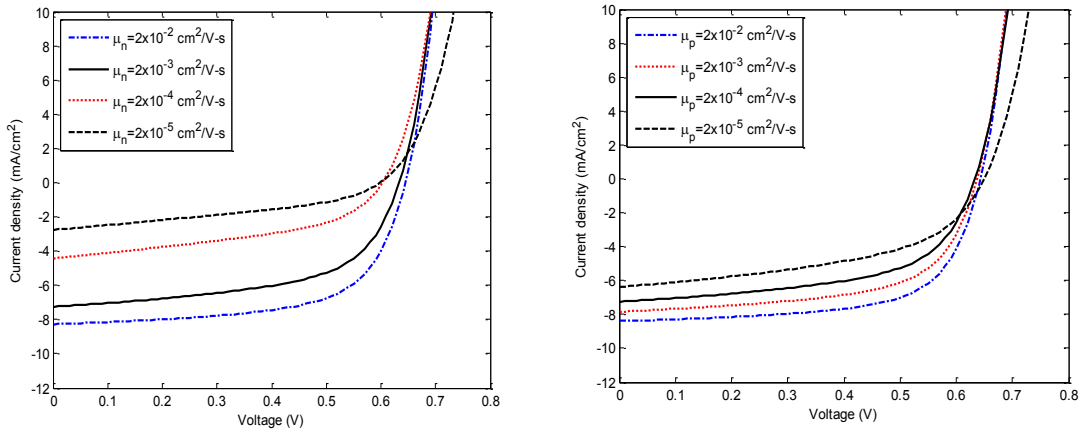

(a) (b)

Figure 4.7 Theoretical current-voltage characteristics of P3HT:PCBM solar cells for (a) varying electron mobility with $\mu_p = 2\times10^{-4}$ cm^2/Vs and (b) varying hole mobility with $\mu_n = 2\times10^{-3}$ cm^2/Vs. Carrier lifetimes are: $\tau_n = 15$ μs and $\tau_p = 10$ μs.

4.4.7 Effects of carrier lifetime on J-V curve

Most of the incident photons are absorbed near the front contact (x = 0) and thus photo-generated free electrons have to travel relatively longer distance than photo-generated holes. Therefore, the efficiency of BHJ solar cells should be more prone to electron lifetime than to hole lifetime. The effects of τ_n and τ_p on the *J-V* characteristics of a 230 nm thick P3HT:PCBM solar cell are shown in Figures 4.8 (a) and (b), respectively. All other parameters in Figure 10 are the same as in Figure 8. The open circuit voltage and short circuit current decrease with decreasing both the electron and hole lifetimes. However, the open circuit voltage is more prone to the electron lifetime whereas the short circuit current is more prone to the hole lifetime. The enhancement of the dark current with decreasing carrier lifetimes reduces the open circuit voltage.

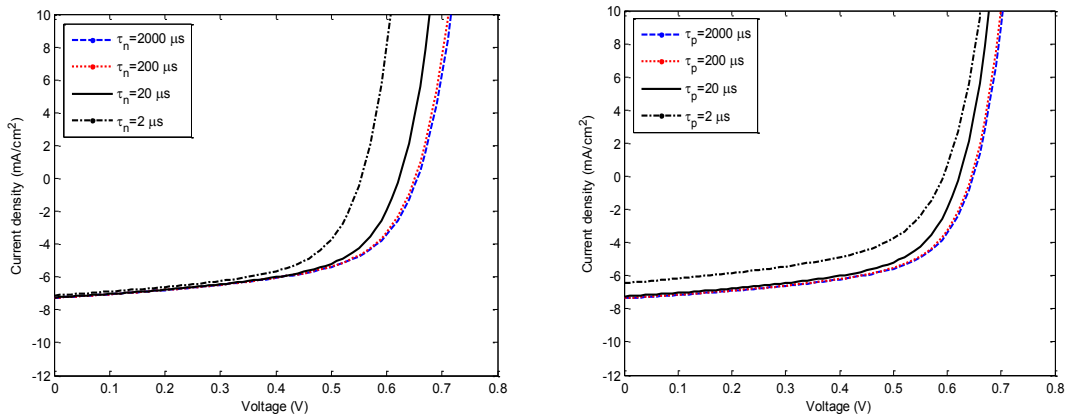

(a) (b)

Figure 4.8 Theoretical current-voltage characteristics of P3HT:PCBM solar cells for (a) varying electron lifetimes with $\tau_p = 20$ μs and (b) varying hole lifetime with $\tau_n = 20$ μs. Carrier mobilities are: $\mu_p = 2\times10^{-4}$ cm^2/Vs and $\mu_n = 2\times10^{-3}$ cm^2/Vs.

4.5 Summary

In this chapter, an analytical photocurrent model has been proposed considering a uniform electric field in the active layer and by solving the continuity equations for both holes and electrons. The net external current is determined by combining the dark current (from chapter 3) and considering the actual solar spectrum. The model is verified by comparing the model calculations with various experimental data. The effects of the contact properties, blend compositions, charge carrier transport properties (carrier mobility and lifetime) and cell design on the overall current-voltage characteristics have been analyzed. The model agrees well with the experimental results.

CHAPTER 5: CONCLUSION, CONTRIBUTION AND FUTURE WORKS

5.1 Conclusion

In this thesis, physics-based mathematical models for the external voltage-dependent forward dark current and photocurrent of BHJ organic solar cells have been developed. The mathematical models are verifield by comparing the model calculations with various published experimental results. The effects of the contact properties, blend compositions, charge carrier transport properties (carrier mobility and lifetime), and cell design on the current-voltage characteristics have been analyzed. The power conversion efficiency of BHJ organic solar cells mostly depends on electron transport properties (both the mobility and lifetime) of the acceptor layer.

The solar cell efficiency also depends on the dissociation efficiency. In this thesis, Modified Braun Model is used to calculate the dissociation efficiency of P3HT:PCBM BHJ organic solar cell. Modified Braun's model shows good agreement with exact extension of Onsager theory at low field. The cell performance improves a lot with the increase in dissociation efficiency which has shown. Again, it has been showed that the cell efficiency is more prone to the electron lifetime than to hole lifetime since electron has to travel relatively longer distance than the holes. Another way to increase the cell performance is annealing. The hole mobility can be improved by annealing which results significant increase in overall efficiency of solar cells based on P3HT:PCBM blend. Besides, if $PC_{71}BM$ is used instead of $PC_{61}BM$ as an acceptor layer, the cell efficiency increases because of the high absorption coefficient of $PC_{71}BM$. Therefore, keeping the same active layer thickness more photo-current can be achievable in $PC_{71}BM$ than in $PC_{61}BM$.

5.2 Contributions and publications

A physics based explicit mathematical model for the external voltage-dependent forward dark current in BHJ organic solar cells has been developed by considering Shockley-Read-

Hall recombination and solving the continuity equations for both electrons and holes. Also, an analytical model for the external voltage-dependent photocurrent in BHJ organic solar cells has been proposed by incorporating exponential photon absorption, dissociation efficiency of bound EHPs, carrier trapping, and carrier drift and diffusion in the photon absorption layer. The following paper is published in a peer-reviewed journal.

- Saleheen, M., Arnab, S. M., & Kabir, M. Z. (2016). Analytical Model for Voltage-Dependent Photo and Dark Currents in Bulk Heterojunction Organic Solar Cells. *Energies*, *9*(6), 412.

This work is also presented as a poster in the following conference,

- M. Mesbahus Saleheen, Salman M. Arnab and M. Z. Kabir , "Analytical model for voltage-dependent photo and dark currents in bulk heterojunction organic solar cells", The 7th International Conference on Optical, Optoelectronic and Photonic Materials and Applications, Polytechnique Montréal, Québec, Canada, June 13-17, 2016.

5.3 Future work

Significant progress can be achieved in OPV device performance by material designing as cell performance depends largely on the optical and electronic properties of the constituents of the active layer. The effective and donor materials can be improved with appropriate band gap and energy levels so that the power can be maximized. Besides, the mobility of charge carriers should be improved. Dissociation efficiency is another great factor in the device performance. It has been shown before that if PCDTBT is used instead of PCBM as an acceptor then the dissociation efficiency goes to almost 99% because PCDTBT is a high dielectric material. High dielectric constant reduces the coulombic attraction between the bound electron and hole. However, the efficiency of PCDTBT is largely depends on the charge transport property i.e. charge collection efficiency. The carrier mobilities are very low in PCDTBT material. Therefore, improving the material properties while considering the dissociation rate is a great challenge for device efficiency.

The work of this thesis provides a complete physics-based model for analyzing the effects of the various controlling parameters on the current voltage characteristics. Thus, this thesis work will provide a quick design tool for optimum solar cell efficiency. Two important assumptions are considered in this thesis. These are (i) uniform electric field and (ii) omission of bimolecular recombination. The precise effects of these two mechanisms can be determined only by simultaneously numerical solution of the Poisson's and continuity equations. This would be the future work of this thesis.

REFERENCES

[1] Grätzel, C., & Zakeeruddin, S. (2013). Recent trends in mesoscopic solar cells based on molecular and nanopigment light harvesters. *Materials Today*, *16*(1-2), 11-18.

[2] Bp.com,. (2015). *Statistical Review of World Energy 2015 | About BP | BP Global*. Retrieved 7 October 2015, from http://bp.com/statisticalreview

[3] Audet, M. (2013). *Why Is Solar Energy Important?*. *LoveToKnow*., from http://greenliving.lovetoknow.com/Why_Is_Solar_Energy_Important

[4] Spanggaard, H., & Krebs, F. C. (2004). A brief history of the development of organic and polymeric photovoltaics. *Solar Energy Materials and Solar Cells*, *83*(2), 125-146.

[5] Goetzberger, A., & Hebling, C. (2000). Photovoltaic materials, past, present, future. *Solar energy materials and solar cells*, *62*(1), 1-19.

[6] Davison, A. (2016). *Common Types of Solar Cells - What are Better Silicon, Monocrystalline, or Polycrystalline Solar Cells?*. *Altenergy.org*. Retrieved from http://www.altenergy.org/renewables/solar/common-types-of-solar-cells.html.

[7] Sbc.slb.com,. (2015). *Solar Photovoltaic*, from https://www.sbc.slb.com/SBCInstitute/Publications/SolarPhotovoltaic.aspx

[8] Mohammad Bagher, A. (2014). Comparison of Organic Solar Cells and Inorganic Solar Cells. *IJRSE*, *3*(3), 53.

[9] Scharber, M., & Sariciftci, N. (2013). Efficiency of bulk-heterojunction organic solar cells. *Progress In Polymer Science*, *38*(12), 1929-1940.

[10] Kumar, P., & Gaur, A. (2013). Model for the JV characteristics of degraded polymer solar cells. *Journal of Applied Physics*, *113*(9), 094505.

[11] Zhang, T., Birgersson, E., & Luther, J. (2013). A spatially smoothed device model for organic bulk heterojunction solar cells. *Journal of Applied Physics*, *113*(17), 174505.

[12] Mihailetchi, V., Koster, L., Hummelen, J., & Blom, P. (2004). Photocurrent Generation in Polymer-Fullerene Bulk Heterojunctions. *Phys. Rev. Lett.*, *93*(21).

[13] Marsh, R., McNeill, C., Abrusci, A., Campbell, A., & Friend, R. (2008). A Unified Description of Current–Voltage Characteristics in Organic and Hybrid Photovoltaics under Low Light Intensity. *Nano Letters*, *8*(5), 1393-1398.

[14] Kumar, P., Jain, S., Kumar, V., Chand, S., & Tandon, R. (2009). A model for the J-V characteristics of P3HT:PCBM solar cells. *J. Appl. Phys.*, *105*(10), 104507.

[15] Altazin, S., Clerc, R., Gwoziecki, R., Pananakakis, G., Ghibaudo, G., & Serbutoviez, C. (2011). Analytical modeling of organic solar cells and photodiodes. *Appl. Phys. Lett.*, *99*(14), 143301.

[16] Schilinsky, P. (2004). Simulation of light intensity dependent current characteristics of polymer solar cells. *J. Appl. Phys.*, *95*(5), 2816.

[17] Blom, P., Mihailetchi, V., Koster, L., & Markov, D. (2007). Device Physics of Polymer:Fullerene Bulk Heterojunction Solar Cells. *Adv. Mater.*, *19*(12), 1551-1566.

[18] Wojcik, M., & Tachiya, M. (2009). Accuracies of the empirical theories of the escape probability based on Eigen model and Braun model compared with the exact extension of Onsager theory. *The Journal Of Chemical Physics*, *130*(10), 104107.

[19] Arnab, S., & Kabir, M. (2014). An analytical model for analyzing the current-voltage characteristics of bulk heterojunction organic solar cells. *J. Appl. Phys.*, *115*(3), 034504.

[20] Chowdhury, M., & Alam, M. (2014). A physics-based analytical model for bulk heterojunction organic solar cells incorporating monomolecular recombination mechanism. *Current Applied Physics*, *14*(3), 340-344.

[21] Street, R., Schoendorf, M., Roy, A., & Lee, J. (2010). Interface state recombination in organic solar cells. *Phys. Rev. B*, *81*(20).

[22] Nolasco, J., Cabré, R., Ferré-Borrull, J., Marsal, L., Estrada, M., & Pallarès, J. (2010). Extraction of poly (3-hexylthiophene) (P3HT) properties from dark current voltage characteristics in a P3HT/n-crystalline-silicon solar cell. *J. Appl. Phys.*, *107*(4), 044505.

[23] Teng, Y., Zhang, Y., Heng, L., Meng, X., Yang, Q., & Jiang, L. (2015). Conductive Polymer Porous Film with Tunable Wettability and Adhesion. *Materials*, *8*(4), 1817-1830.

[24] Thompson, B. & Fréchet, J. (2008). Polymer–Fullerene Composite Solar Cells. *Angewandte Chemie International Edition*, *47*(1), 58-77

[25] Hou, J., & Guo, X. (2012). Active Layer Materials for Organic Solar Cells. *Organic Solar Cells*, 17-42.

[26] Lenes, M., Shelton, S., Sieval, A., Kronholm, D., Hummelen, J., & Blom, P. (2009). Electron Trapping in Higher Adduct Fullerene-Based Solar Cells. *Adv. Funct. Mater.*, *19*(18), 3002-3007.

[27] Yoo, S., Kum, J., & Cho, S. (2011). Tuning the electronic band structure of PCBM by electron irradiation. *Nanoscale Res Lett*, *6*(1), 545.

[28] Kim, Y., Choulis, S., Nelson, J., Bradley, D., Cook, S., & Durrant, J. (2005). Composition and annealing effects in polythiophene/fullerene solar cells. *J Mater Sci*, *40*(6), 1371-1376.

[29] Lu, Y., Wang, Y., Feng, Z., Ning, Y., Liu, X., Lü, Y., & Hou, Y. (2012). Temperature-dependent morphology evolution of P3HT:PCBM blend solar cells during annealing processes. *Synthetic Metals*, *162*(23), 2039-2046.

[30] Baumann, A., Lorrmann, J., Rauh, D., Deibel, C., & Dyakonov, V. (2012). A New Approach for Probing the Mobility and Lifetime of Photogenerated Charge Carriers in Organic Solar Cells Under Real Operating Conditions. *Adv. Mater.*, *24*(32), 4381-4386.

[31] Garcia-Belmonte, G., Munar, A., Barea, E., Bisquert, J., Ugarte, I., & Pacios, R. (2008). Charge carrier mobility and lifetime of organic bulk heterojunctions analyzed by impedance spectroscopy. *Organic Electronics*, *9*(5), 847-851.

[32] Tremolet de Villers, B., Tassone, C., Tolbert, S., & Schwartz, B. (2009). Improving the Reproducibility of P3HT:PCBM Solar Cells by Controlling the PCBM/Cathode Interface. *J. Phys. Chem. C*, *113*(44), 18978-18982.

[33] Monestier, F., Simon, J., Torchio, P., Escoubas, L., Flory, F., & Bailly, S. et al. (2007). Modeling the short-circuit current density of polymer solar cells based on P3HT:PCBM blend. *Solar Energy Materials And Solar Cells*, *91*(5), 405-410.

[34] Mihailetchi, V., Xie, H., de Boer, B., Koster, L., & Blom, P. (2006). Charge Transport and Photocurrent Generation in Poly(3-hexylthiophene): Methanofullerene Bulk-Heterojunction Solar Cells. *Adv. Funct. Mater.*, *16*(5), 699-708.

[35] Gregg, B., & Hanna, M. (2003). Comparing organic to inorganic photovoltaic cells: Theory, experiment, and simulation. *J. Appl. Phys.*, *93*(6), 3605.

[36] Mayer, A., Scully, S., Hardin, B., Rowell, M., & McGehee, M. (2007). Polymer-based solar cells. *Materials Today*, *10*(11), 28-33.

[37] Brütting, W. (2005). Introduction to the Physics of Organic Semiconductors. *BRUETTING:ORG.SEMICONDUCT O-BK*, 1-14.

[38] Coakley, K., & McGehee, M. (2004). Conjugated Polymer Photovoltaic Cells. *Chemistry Of Materials*, *16*(23), 4533-4542.

[39] *Solar Spectral Irradiance: ASTM G-173*. (2016). *Rredc.nrel.gov*. Retrieved from http://rredc.nrel.gov/solar/spectra/am1.5/astmg173/astmg173.html

[40] Nunzi, J. (2002). Organic photovoltaic materials and devices. *Comptes Rendus Physique*, *3*(4), 523-542.

[41] Scharber, M., Mühlbacher, D., Koppe, M., Denk, P., Waldauf, C., Heeger, A., & Brabec, C. (2006). Design Rules for Donors in Bulk-Heterojunction Solar Cells—Towards 10 % Energy-Conversion Efficiency. *Adv. Mater.*, *18*(6), 789-794.

[42] Mihailetchi, V., Blom, P., Hummelen, J., & Rispens, M. (2003). Cathode dependence of the open-circuit voltage of polymer:fullerene bulk heterojunction solar cells. *J. Appl. Phys.*, *94*(10), 6849.

[43] Xie, F., Choy, W., Wang, C., Sha, W., & Fung, D. (2011). Improving the efficiency of polymer solar cells by incorporating gold nanoparticles into all polymer layers. *Appl. Phys. Lett.*, *99*(15), 153304.

[44] Peng, B., Guo, X., Cui, C., Zou, Y., Pan, C., & Li, Y. (2011). Performance improvement of polymer solar cells by using a solvent-treated poly(3,4-ethylenedioxythiophene):poly(styrenesulfonate) buffer layer. *Appl. Phys. Lett.*, *98*(24), 243308.

[45] Shrotriya, V., Li, G., Yao, Y., Moriarty, T., Emery, K., & Yang, Y. (2006). Accurate Measurement and Characterization of Organic Solar Cells. *Adv. Funct. Mater.*, *16*(15), 2016-2023.

[46] Sidi, P., Sukoco, D., Purnomo, W., Sudibyo, H., & Hartanto, D. (2013). Electric Energy Management and Engineering in Solar Cell System. *Solar Cells - Research And Application Perspectives*.

[47] Sokel, R. (1982). Numerical analysis of transient photoconductivity in insulators. *J. Appl. Phys.*, *53*(11), 7414.

[48] Deibel, C., Dyakonov, V., & Brabec, C. (2010). Organic Bulk-Heterojunction Solar Cells. *IEEE J. Select. Topics Quantum Electron.*, *16*(6), 1517-1527.

[49] Namkoong, G., Kong, J., Samson, M., Hwang, I., & Lee, K. (2013). Active layer thickness effect on the recombination process of PCDTBT:PC71BM organic solar cells. *Organic Electronics*, *14*(1), 74-79.

[50] Shuttle, C. G., O'Regan, B., Ballantyne, A. M., Nelson, J., Bradley, D. D. C., De Mello, J., & Durrant, J. R. (2008). Experimental determination of the rate law for charge carrier decay in a polythiophene: Fullerene solar cell. *Applied Physics Letters*, *92*(9), 3311.

[51] Mandoc, M. M., Kooistra, F. B., Hummelen, J. C., De Boer, B., & Blom, P. W. M. (2007). Effect of traps on the performance of bulk heterojunction organic solar cells. *Applied Physics Letters*, *91*(26), 263505.

[52] Hernández-García, L., Cabrera-Arenas, V., & Reséndiz-Mendoza, L. (2015). On the convergence of the algorithm for simulating organic solar cells. *Computer Physics Communications*, *196*, 372-379.

[53] Shuttle, C., Hamilton, R., O'Regan, B., Nelson, J., & Durrant, J. (2010). Charge-density-based analysis of the current-voltage response of polythiophene/fullerene photovoltaic devices. *Proceedings Of The National Academy Of Sciences*, *107*(38), 16448-16452.

[54] Chowdhury, M., & Alam, M. (2015). An optoelectronic analytical model for bulk heterojunction organic solar cells incorporating position and wavelength dependent carrier generation. *Solar Energy Materials And Solar Cells*, *132*, 107-117.

[55] Sze, S. (1985). *Semiconductor devices, physics and technology*. New York: Wiley.

[56] Solanki, C. (2011). *Solar Photovoltaics: Fundamentals, Technologies and Applications* (2nd ed.).

[57] Kirchartz, T., Pieters, B., Kirkpatrick, J., Rau, U., & Nelson, J. (2011). Recombination via tail states in polythiophene:fullerene solar cells. *Phys. Rev. B*, *83*(11).

[58] Koster, L., Mihailetchi, V., Ramaker, R., & Blom, P. (2005). Light intensity dependence of open-circuit voltage of polymer:fullerene solar cells. *Appl. Phys. Lett.*, *86*(12), 123509.

[59] Rauh, D., Deibel, C., & Dyakonov, V. (2012). Charge density dependent nongeminate recombination in organic bulk heterojunction solar cells. *Advanced Functional Materials*, *22*(16), 3371-3377.

[60] Servaites, J. D., Ratner, M. A., & Marks, T. J. (2011). Organic solar cells: a new look at traditional models. *Energy & Environmental Science*, *4*(11), 4410-4422.

[61] Taretto, K., Rau, U., & Werner, J. (2003). Closed-form expression for the current/ voltage characteristics of pin solar cells. *Applied Physics A: Materials Science & Processing*, *77*(7), 865-871.

[62] Rredc.nrel.gov,. (2015). *Solar Spectral Irradiance: Air Mass 1.5*. Retrieved 6 November 2015

[63] Braun, C. L. (1984). Electric field assisted dissociation of charge transfer states as a mechanism of photocarrier production. *The Journal of chemical physics*, *80*(9), 4157-4161.

[64] Nelson, J. (2003). *The physics of solar cells*. London: Imperial College Press.

[65] Anjan, M., & Kabir, M. (2011). Modeling of current-voltage characteristics of CdS/CdTe solar cells. *Phys. Status Solidi A*, *208*(8), 1813-1816.

[66] Kasap, S.O. (2013) Optoelectronics and Photonics: Principles of Practices, 2nd Edition, New Jersey: Pearson Education, Ch. 5.

[67] Park, S. H., Roy, A., Beaupre, S., Cho, S., Coates, N., Moon, J. S., ... & Heeger, A. J. (2009). Bulk heterojunction solar cells with internal quantum efficiency approaching 100&percnt. *nature photonics*, *3*(5), 297-302.

[68] Koster, L. J. A., Smits, E. C. P., Mihailetchi, V. D., & Blom, P. W. M. (2005). Device model for the operation of polymer/fullerene bulk heterojunction solar cells. *Physical Review B*, *72*(8), 085205.

[69] Monestier, F., Simon, J. J., Torchio, P., Escoubas, L., Flory, F., Bailly, S., ... & Defranoux, C. (2007). Modeling the short-circuit current density of polymer solar cells based on P3HT: PCBM blend. *Solar energy materials and solar cells*, *91*(5), 405-410.

[70] Sandberg, O. J., Nyman, M., & Österbacka, R. (2014). Effect of contacts in organic bulk heterojunction solar cells. *Physical Review Applied*, *1*(2), 024003.